

## Torin 1 alleviates impairment of TFEB-mediated lysosomal biogenesis and autophagy in *TGFBI* (p.G623\_H626del)-linked Thiel-Behnke corneal dystrophy

Liyuan Wang <sup>a\*</sup>, Chuchu Zhao <sup>a\*</sup>, Tao Zheng <sup>a\*</sup>, Yi Zhang<sup>a\*</sup>, Hanruo Liu<sup>b\*</sup>, Xi Wang<sup>a</sup>, Xianling Tang<sup>a</sup>, Baowen Zhao<sup>a</sup>, and Ping Liu<sup>a</sup>

<sup>a</sup>Department of Ophthalmology, The First Affiliated Hospital of Harbin Medical University, Harbin, China; <sup>b</sup>The Beijing Institute of Ophthalmology, Beijing Tongren Hospital, Capital Medical University, Beijing, China

### ABSTRACT

Thiel-Behnke corneal dystrophy (TBCD) is an epithelial-stromal *TGFBI* dystrophy caused by mutations in the *TGFBI* (transforming growth factor beta induced) gene, though the underlying mechanisms and pathogenesis of TBCD are still obscure. The study identifies a novel mutation in the *TGFBI* gene (p.Gly623\_His626del) in a TBCD pedigree. Characteristics of the typical vacuole formation, irregular corneal epithelial thickening and thinning, deposition of eosinophilic substances beneath the epithelium, and involvement of the anterior stroma were observed in this pedigree via transmission electron microscopy (TEM) and histological staining. *Tgfb1*-p.Gly623\_Tyr626del mouse models of TBCD were subsequently generated via CRISPR/Cas9 technology, and the above characteristics were further verified via TEM and histological staining. Lysosomal dysfunction and downregulation of differential expression protein CTSD (cathepsin D) were observed using LysoTracker Green DND-26 and proteomic analysis, respectively. Hence, lysosomal dysfunction probably leads to autophagic flux obstruction in TBCD; this was supported by enhanced LC3-II and SQSTM1 levels and decreased CTSD. TFEB (transcription factor EB) was prominently decreased in TBCD corneal fibroblasts and administration of ATP-competitive MTOR inhibitor torin 1 reversed this decline, resulting in the degradation of accumulated mut-TGFBI (mutant TGFBI protein) via the ameliorative lysosomal function and autophagic flux owing to elevated TFEB activity as measured by western blot, confocal microscopy, and flow cytometry. Transfected HEK 293 cells overexpressing human full-length WT-*TGFBI* and mut-*TGFBI* were generated to further verify the results obtained in human corneal fibroblasts. Amelioration of lysosome dysfunction may therefore have therapeutic efficacy in the treatment of TBCD.

**Abbreviations** AS-OCT: anterior segment optical coherence tomography; ATP: adenosine triphosphate; Cas9: CRISPR-associated protein 9; CLEAR: coordinated lysosomal expression and regulation; CRISPR: clustered regularly interspaced short palindromic repeats; CTSB: cathepsin B; CTSD: cathepsin D; CTSF: cathepsin F; CTSL: cathepsin L; DNA: deoxyribonucleic acid; ECM: extracellular matrix; Fas1: fasciclin 1; FC: flow cytometry; GAPDH: glyceraldehyde-3-phosphate dehydrogenase; GCD2: granular corneal dystrophy type 2; HE: hematoxylin and eosin; LAMP2: lysosomal-associated membrane protein; MT: mutation type; MTOR: mechanistic target of rapamycin kinase; MTORC1: MTOR complex 1; mut-TGFBI: mutant TGFBI protein; SD: standard deviation; TBCD: Thiel-Behnke corneal dystrophy; TEM: transmission electron microscopy; TFEB: transcription factor EB; TGFBI: transforming growth factor beta induced; WT: wild type

### ARTICLE HISTORY

Received 24 October 2020  
Revised 5 July 2021  
Accepted 7 July 2021

### KEYWORDS

Autophagy; lysosome dysfunction; TBCD; TFEB; *TGFBI*; torin 1

### Introduction


Lysosomes are dynamic organelles that control the switch between anabolism and catabolism by regulating lysosomal biogenesis and macroautophagy/autophagy (herein referred to as autophagy) [1,2]. Generally speaking, lysosomes are the terminal degradative components of the autophagy–lysosomal pathways [3]. The regulation of lysosomal function and the succedent process of protein degradation depends on numerous factors; foremost among these are proteolytic enzyme activity and luminal pH [4]. Cathepsins are proteases contained in lysosomes and are essential for many biological processes, including digestion, immune response, and peptide synthesis. Cathepsins consist primarily of 15 classes and have

the capacity to hydrolyze proteins delivered to endolysosomes [5]. CTSD is a representative aspartic proteinase responsible for the maintenance of cellular proteostasis and the intra-lysosomal digestion of autophagic material. Two enzymatically active forms of CTSD have been revealed: 1) a single-chain form that is rapidly converted into the double-chain form that is active at a very acidic pH of 5.5–6.5 within the endosomes and 2) a mature double-chain form that is active at a pH of 3.5–4.5 within the lysosomes [6]. The latter form participates in the autophagy-lysosome protein degradation pathway, showing a particular affinity for substrates enriched in hydrophobic (aromatic) amino acids [7]. Previous studies have reported that the lack of CTSD in mice results in a severe

**CONTACT** Ping Liu  [ping\\_liu53@hotmail.com](mailto:ping_liu53@hotmail.com)  Department of Ophthalmology, The First Affiliated Hospital of Harbin Medical University, Harbin China

\*These authors contributed equally to this work.

This article has been republished with minor changes. These changes do not impact the academic content of the article.

 Supplemental data for this article can be accessed [here](#)

© 2021 The Author(s). Published by Informa UK Limited, trading as Taylor & Francis Group.

This is an Open Access article distributed under the terms of the Creative Commons Attribution-NonCommercial-NoDerivatives License (<http://creativecommons.org/licenses/by-nc-nd/4.0/>), which permits non-commercial re-use, distribution, and reproduction in any medium, provided the original work is properly cited, and is not altered, transformed, or built upon in any way.

blockage of the autophagic flux and that the activity of CTSD is essential for degrading the unfolded protein aggregates delivered to lysosomes via autophagy and endocytosis [6].

The regulation of lysosomal gene expression depends on the coordinated lysosomal expression and regulation (CLEAR) network, which is recognized by its master regulator TFEB [8]. TFEB was the first member in the MiTF/TFE family to be identified as a master regulator of lysosomal biogenesis and is primarily regulated by the MTOR (mechanistic target of rapamycin kinase) complex 1 (MTORC1). Specifically, the activated form of TFEB participates in a number of biological processes involved in cellular clearance, including lysosomal biogenesis, autophagy, exocytosis, and endocytosis [9]. The lysosomal hydrolases that participate in substrate degradation, such as CTSD, belong to the group identified as transcriptional targets of TFEB [10]. Previous studies have shown that, under basal conditions, a substantial fraction of TFEB is phosphorylated by MTOR on S142 and S211 serine residues and the binding of YWHA/14-3-3 proteins is retained in the cytoplasm [11,12]. However, upon starvation or lysosomal stress, TFEB is activated following dephosphorylation and is translocated to the nucleus by inhibition of MTOR and concomitant activation of the phosphatase PPP3/calcineurin [13].

*TGFBI* gene-linked corneal dystrophies (CD)s are a group of primary inherited progressive corneal diseases. The typical clinical manifestation of CD is a gradual loss of corneal transparency in bilateral eyes, which often leads to recurrent corneal erosion and visual impairment. TGFBI is an extracellular matrix (ECM) protein with a secretory signal sequence and cysteine-rich domain at the N terminus, four homologous internal Fas1 (fasciclin 1) domains, and an Arg-Gly-Asp (RGD) integrin recognition sequence at the C-terminus [14,15]. Progressive abnormal aggregation of mut-TGFBI deposits in the corneal epithelia and stroma that interfere with corneal transparency, thus impairing visual acuity, is the hallmark of *TGFBI*-linked CDs. *In vitro* studies have shown that TGFBI mediates cell growth, cell differentiation, wound healing, cell adhesion, migration [16], apoptosis [17], proliferation, and tumorigenesis. Furthermore, TGFBI mediates migration and cell adhesion through interaction with cell surface integration in receptors [18]. TFEB has been explored as a potential therapy target in some lysosomal storage diseases that are distinguished by aberrant protein accumulation and the impairment of the autophagy-lysosomal process. However, the mechanisms involved in corneal diseases, especially CDs, remain elusive.

Thiel-Behnke corneal dystrophy (TBCD; OMIM 602082) is a *TGFBI*-linked CD that is characterized by honeycomb-like, subepithelial corneal opacities with recurrent erosions. It appears in the first and second decades of life and was categorized as an “epithelial-stromal *TGFBI* dystrophy” by the International Committee for Classification of Corneal Dystrophies (IC3D) in 2015 [19]. TBCD has been mapped to chromosome 5q31 of *TGFBI* and is associated with the following mutations: p.M502V/R555Q, p.R555Q and p.H626P [20–23]. Lesions related to TBCD predominantly occur in the surface epithelium, the Bowman membrane/anterior basement membrane complex and the subepithelium, as well as the anterior stroma of the cornea. Lesions related to TBCD predominantly occur in the Bowman

layer and the subepithelium. They also occur in the surface epithelium, Bowman membrane–anterior basement membrane complex, and the anterior stroma of the cornea. Irregular deposits within the epithelium and the Bowman layer, as detected by confocal microscopy and anterior segment optical coherence tomography (AS-OCT) and the substitution of electron-dense bodies by “curly fibers,” as observed by electron microscopy of corneal tissue can be used to help diagnose TBCD [24,25].

Autophagy is the main intracellular lysosome-dependent degradation mechanism for TGFBI and a defect in autophagy could be related to the mut-TGFBI aggregates in *TGFBI*-linked corneal fibroblasts in granular corneal dystrophy type 2 (GCD2) [26]. However, in other *TGFBI*-linked corneal dystrophies such as TBCD, the underlying mechanisms and pathogenesis remain ambiguous, regardless of available therapies or drugs.

In this study, we identified a novel association between TBCD and the *TGFBI* (p.Gly623\_His626del) mutation and analyzed the severity of clinical and pathological phenotype at different stages of keratopathy. It was found that lysosomal alkalization and downregulation of CTSD may contribute to the obstruction of autophagic flux in *TGFBI* (p.Gly623\_His626del) TBCD. We hypothesize that impaired lysosomal function, resulting from lysosomal alkalization and CTSD deficiency might be responsible for the defective degradation of mut-TGFBI as a result of autophagy flux blockage in TBCD. Torin 1 largely promoted the degradation of mut-TGFBI by activating TFEB-mediated transcription of lysosome and autophagy-related genes. These findings provide new insights into the pathogenic mechanisms of *TGFBI* gene mutations in (p.Gly623\_His626del)-linked TBCD and suggest that correcting lysosome dysfunction by pharmacological modulation of TFEB activity may represent a promising therapeutic avenue.

## Results

### *The diagnosis of TBCD in a family with p.Gly623\_His626del mutation of the TGFBI gene*

Fourteen individuals from a five-generation pedigree were recruited, including seven affected and seven unaffected members (Figure 1A). All of the affected patients had one parent that suffered from corneal dystrophy, indicating that the pathogenic gene was transmitted from the parent and suggesting autosomal dominant inheritance. The proband of this family (III-6) was a 49-year-old man who began to experience repeated irritative eye symptoms at a young age, but did not seek medical advice due to the limited availability of local medical services. Visual acuity deteriorated and corneal lesions increased as the disease progressed with age in the proband and in other affected family members. All clinical information is listed in Table S1. Slit-lamp examination of patient IV-6 revealed bilateral tiny, superficial, irregularly shaped gray “honeycomb” opacities as shown by the arrow in the area of the pupil. The peripheral cornea had more irregular diffuse opacities with clear interruptions that extended to the limbus in RBCD (Figure 1B). Patient IV-4 exhibited an extensive

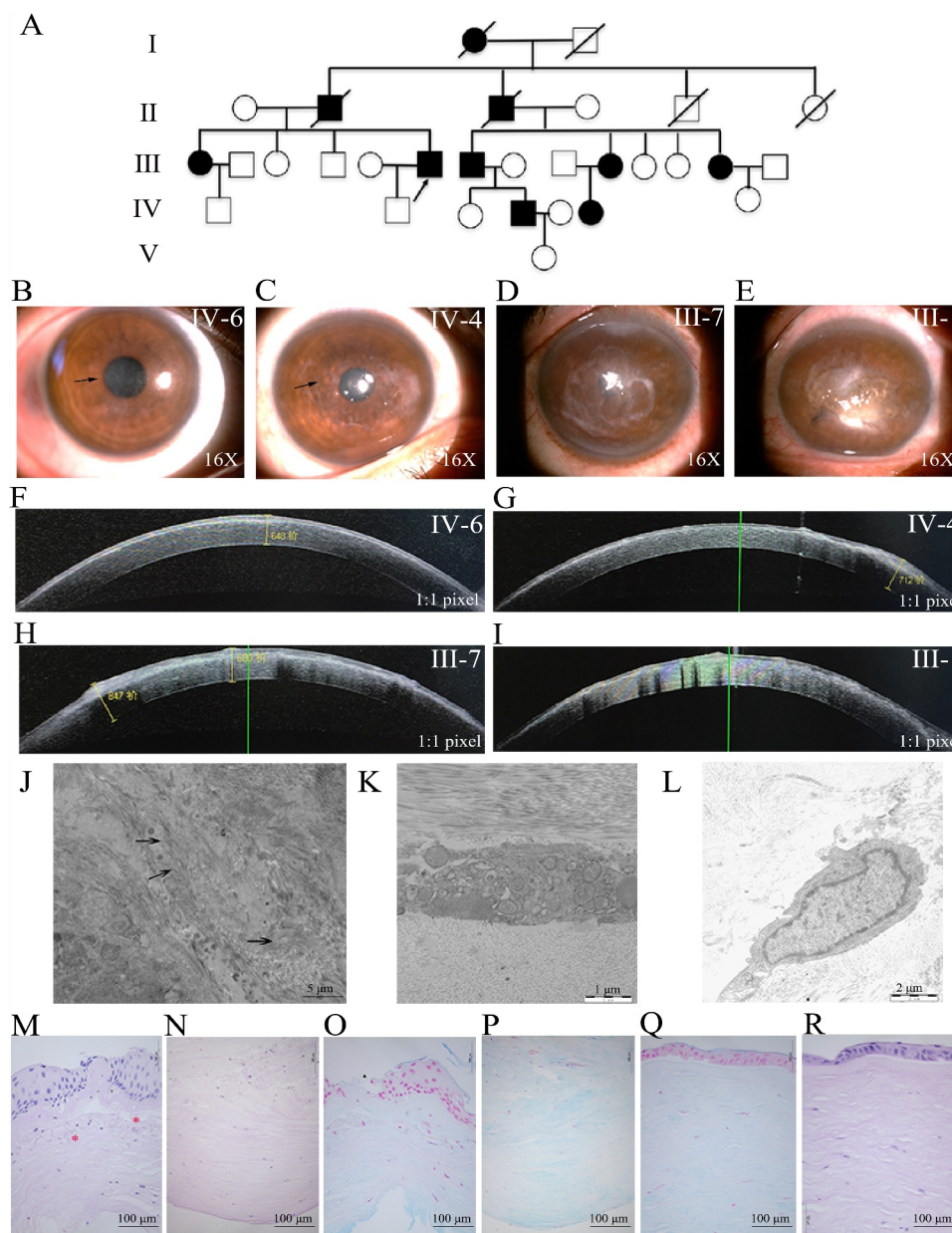


**Figure 1.** Phenotypes and histopathological observation of a TBCD family with p.Gly623\_His626del mutation of the *TGFBI* gene. (A) Pedigree showing inheritance of TBCD. The proband of the family is highlighted with an arrow. Open and closed symbols indicate unaffected and affected individuals, respectively. Deceased family members are denoted by diagonal slashes. (B–E) Slit-lamp photographs showing progression of the disease from minor to serious. Irregularly shaped gray “honeycomb” opacities were observed (black arrow) in IV-6 and IV-4 in the pupil area with noninvolvement of the peripheral cornea in the Bowman layer in (B) and (C). Slit-lamp photographs of III-7 and III-1 show a mass of gray-white opacities, progressing to the corneal periphery and secondary scarring in (D) and (E). The corresponding AS-OCT results are shown in (F–I). The typical hyperreflective, thick-banded lesion with a saw-tooth pattern toward the corneal epithelium in Bowman’s layer was observed. (J) The presence of curly collagen fibers (black arrow) in MT corneal tissues by TEM. (K) TEM shows numerous vacuole formations, impairment of cellular integrity, increase in autophagosomes, and abnormal lysosomes in MT corneal stroma compared with normal corneal stroma structure in WT corneal tissues in (L). (M–N) and (O–P) respectively show histologic features of MT corneal tissues by HE staining and Alcian blue stain. (M) shows the irregular changes of corneal epithelium and the eosinophilic deposits (asterisks) beneath the epithelium, involved the anterior stroma in MT by HE. (O) Alcian blue stain shows the sawtooth-like appearance of Bowman layer and the partial absence of the basement membrane in MT. (N, P) The uninvolved deeper corneal stromal layer in MT. (Q–R) HE staining and Alcian blue staining of WT corneal tissues (scale bars: 16X in B–E; 1:1 pixel in F–I; 5  $\mu$ m in J; 1  $\mu$ m in K; 2  $\mu$ m in L; 100  $\mu$ m in M–R).

honeycomb-shaped configuration of grayish opacities beneath the epithelium and at the Bowman’s layer (Figure 1C). As the disease worsened with age, the opacities progressed from the central cornea to the periphery and presented with a large gray-white opacity and secondary scar tissue instead of typical honeycomb opacities as observe via slit-lamp examination of patients III-7 and III-1 (Figure 1D,E).

AS-OCT showed a hyperreflective and continuous thin band in Bowman’s layer in patient IV-6 (Figure 1F) and a partial, thick-banded lesion toward the corneal epithelium that was consistent with the lesions observed via slit-lamp in patient IV-4 (Figure 1G). A hyperreflective, thick-banded lesion with a saw-toothed pattern was observed toward the corneal epithelium in Bowman’s layer via AS-OCT examination in the eyes of patients III-7 and III-1 (Figure 1H,I).

TEM seemed to be the best means for diagnosing, distinguishing and differentiating different patterns of sediment. Presence of curly collagen fibers, as opposed to the rod-shaped electron-dense bodies in the excised corneal tissue of the mutation type (MT, which hereinafter refers to the p. Gly623\_His626del team), was slightly visible, as shown by the arrow in Figure 1J, and was an important characteristic to distinguish this from RBCD. Moreover, TEM observations of corneal fibroblasts confirmed that TBCD corneal fibroblasts exhibited a series of vacuole formations, impairment of cellular integrity, accumulations of double-membrane structure, and abnormally enlarged lysosomes as contrasted to wild type (WT) (Figure 1K,L). Hematoxylin and eosin (HE) staining analysis of MT corneal tissues demonstrated an irregularly thickened and thinned layered corneal epithelium, eosinophilic deposits (shown by asterisks) beneath the epithelium, and involvement of the anterior stroma compared to normal cornea (Figure 1M,N). The Bowman layer had a characteristic sawtooth-like appearance and a focal absence of the epithelial basement membrane that was replaced by

superficial fibrosis, which caused alternating irregular thickening and thinning of the epithelial layer as shown by Alcian blue dye (Figure 1O,P). The deeper corneal stromal layer, Descemet's membrane, and endothelium appeared to be normal in MT (Figure 1N,P) and consistent with WT (Figure 1Q, R), as demonstrated using two dyeing methods.

Mutated variant analysis and Sanger sequencing detected a heterozygous c.1868–1879del mutation, resulting in an in-frame mutation in the affected members of this family, which was absent in unaffected members (Figure 2A,B). This heterozygous involves deletion of twelve nucleotides of exon 14, causing an in-frame mutation, resulting in deletion of four amino acids (GVVH) and leading to connection of adjacent residual amino acids (Figure 2C). Even though the effect of the mutation on the physicochemical properties of the TGFBI remains unclear, attempts to describe the structural modification for mutations in the Fas1-4 domain will be touched upon briefly. To predict the possible effects of TGFBI structure, a protein model was established to exhibit variations associated with mutations in the Fas1-4 domain (Figure 2D). The

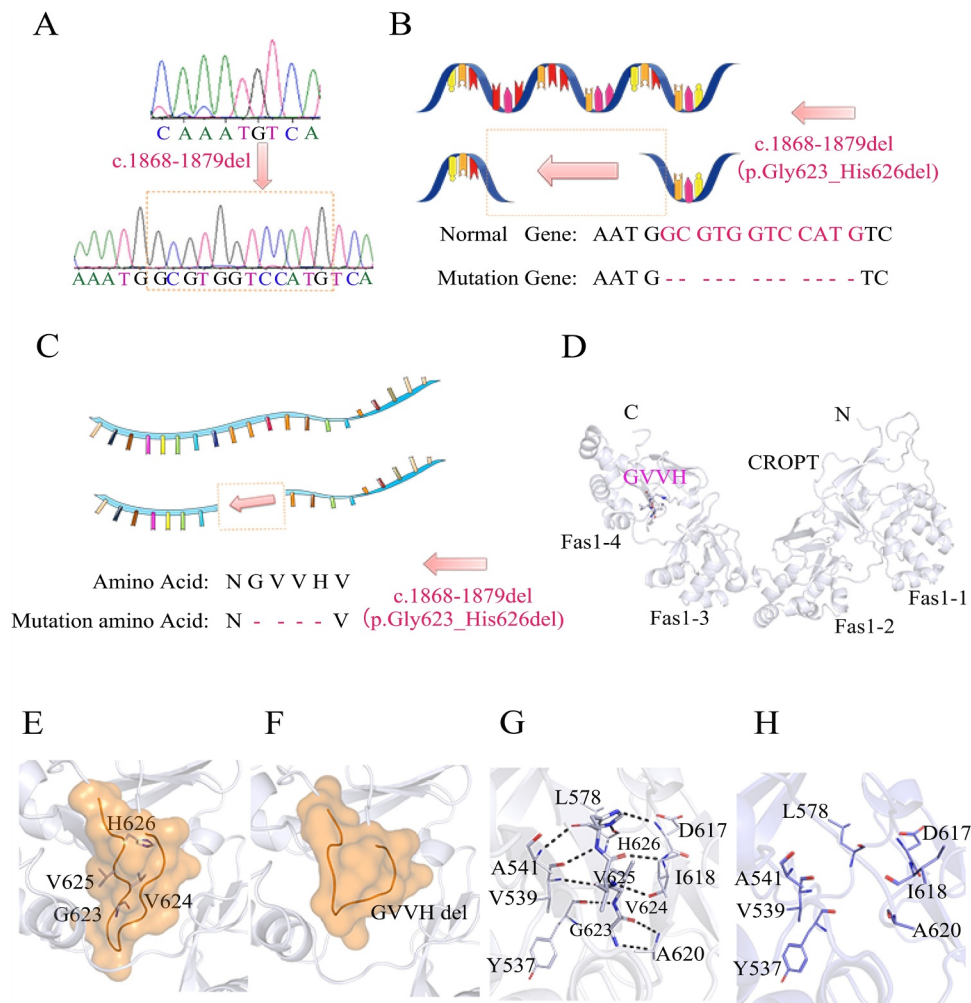


**Figure 2.** Sequence analysis of the mutated *TGFBI* gene and the probable modification for the c.1868–1879del in the Fas1-4 domain involved in the mut-TGFBI structure. (A) Sequence chromatograms show the novel heterozygous deletion mutation (c.1868–1879del). (B) Shows the normal sequence of *TGFBI* and the mutated sequence. (C) Shows the normal corresponding amino acid sequence and the mutated amino acid sequence below with lack of GVVH and the repaired connect after the deletion. (D) Shows the human WT-TGFBI structure containing four fasciclin 1 domains. The mut-TGFBI structure exhibits the deletion of four amino acid (GVVH). (E-F) Secondary structure of TGFBI changed from the stabilized state of  $\beta$ -sheet to a flexible loop region resulting from the c.1868–1879del. (G-H) Before mutation: GVVH formed a dense hydrogen bond system with surrounding amino acids, which stabilized the local structure and played a conclusive role in regional stability and conformation. After mutation: GVVH deletion system, the surrounding amino acid hydrogen bond network system disappeared.

conformational conversion from the stabilized state of  $\beta$ -sheet to a flexible loop region (Figure 2E,F) caused the disappearance of the surrounding amino acid hydrogen bond network system leading to the changes in its physical and chemical properties (Figure 2G,H).

Based on the above data, including clinical features, AS-OCT images, and histopathologic analysis, the corneal dystrophy in this family was preliminarily diagnosed as TBCD.

### Abnormal corneal characterization of *Tgfb1-p.Gly623\_Tyr626del* mice

To better elucidate the effect of the *Tgfb1* mutation on the development and progression of TBCD, CRISPR-Cas9 technology was used to generate a *Tgfb1-p.Gly623\_Tyr626del* mouse model of TBCD. The relevant sgRNAs and the specific location in exon 14 are shown in Figure 3A,B. DNA sequencing technology was conducted to identify the *Tgfb1-p.Gly623\_Tyr626del* mutant mice and to further examine the genotype of the pups (Figure 3C). Somewhat surprisingly, upon slit-lamp examination, the *Tgfb1-p.Gly623\_Tyr626del* mice had corneal opacities, similar to human TBCD patients when compared with wild-type mice (Figure 3D). In addition, electron-dense deposits in the corneal fibroblasts and extracellular matrix, as well as formation of vacuolated cytoplasm was observed via TEM in 42 week-old mice (Figure 3E,F). HE staining demonstrated irregular thickening and thinning of the corneal epithelia of *Tgfb1<sup>Gly623\_Tyr626del</sup>/WT* mice compared with WT *Tgfb1* mice (Figure 3G). Protein modeling of mouse TGFBI structure revealed a minor variation in the overall geometry of the protein (Fig. S1A and S1B) in MT compared with WT mice. Structure in MT mice was similar to the structure of human TGFBI, in which the stabilized  $\beta$ -sheet had a flexible loop region resulting from the lack of GVVY (Fig. S1C and S1D). The corresponding hydrogen bond network system was not present, leading to the modification of physical and chemical properties of TGFBI (Fig. S1E and S1F).

### Autophagic flux was obstructed in TBCD corneal fibroblasts

Because the expression of TGFBI was distinctly upregulated in TBCD corneal fibroblasts compared with WT corneal fibroblasts as shown by western blotting (Figure 4A,B), the levels of *TGFBI* mRNA between WT and MT corneal fibroblasts were compared using real-time PCR, to determine whether *TGFBI* mRNA was upregulated in TBCD corneal fibroblasts. As shown in Figure 4C, no significant differences in expression levels of total *TGFBI* mRNA were detected between WT and MT corneal fibroblasts. Although the total *TGFBI* mRNA abundance was comparable between WT and MT corneal fibroblasts, the WT-*TGFBI* mRNA abundance was markedly lower in MT corneal fibroblasts than in WT corneal fibroblasts (Figure 4D). Due to the heterozygous mutation of *TGFBI* in MT corneal fibroblasts, the levels of TGFBI and WT-*TGFBI* mRNA were evaluated in MT corneal fibroblasts and it was found that mut-TGFBI accumulated in TBCD corneal fibroblasts.

In eukaryotic cells, two main cellular protein degradation pathways are responsible for the removal of abnormal proteins: one is the ubiquitin/proteasome pathway and the other is the autophagy pathway [27]. To explore whether the ubiquitin/proteasome pathway contributes to mut-TGFBI degradation in TBCD, western blotting was conducted with ubiquitins. As expected, there were no remarkable differences in ubiquitin levels between WT and MT corneal fibroblasts, with equal loading verified by Coomassie Brilliant Blue staining (Fig. S2). The above observations indicate that no significant change in ubiquitin/proteasome pathways were found in TBCD corneal fibroblasts. LAMP2 (lysosomal-associated membrane protein 2) is mainly wrapped around the inner surface of the lysosomal membrane and localized in late endosomes and lysosomes. LAMP2 is responsible for the degradation of cytosolic proteins in the lysosome [24]. Confocal microscopy revealed that TGFBI puncta had colocalized with LAMP2 in cytosolic vesicles in both WT and MT as shown in Figure 4E, indicating that TGFBI might be trafficked to lysosomes in TBCD corneal fibroblasts and that mut-TGFBI may be degraded in the lysosome. In addition, TBCD heterozygous corneal fibroblasts revealed a much more extensive pattern of mut-TGFBI colocalized with LAMP2 than was observed in WT corneal fibroblasts (Figure 4F). This finding suggests that, in TBCD, accumulated mut-TGFBI in corneal fibroblasts might predominantly be degraded in lysosomes. Previous reports have confirmed that autophagy is mainly responsible for TGFBI degradation in GCD2 corneal dystrophy [26]. Hence, the following analyses and TEM data examine whether there are pathological changes in the autophagy-lysosomal pathway in TBCD corneal fibroblasts.

To examine autophagy activity in TBCD corneal fibroblasts, the protein levels of the autophagosomal protein, LC3 and the autophagy substrate protein, SQSTM1 were detected. The levels of LC3-II and SQSTM1 were significantly increased in MT corneal fibroblasts compared to WT corneal fibroblasts (Figure 4G,H). These data suggest that autophagic flux is obstructed in TBCD corneal fibroblasts.

We speculated that the possible reasons for the blockage of autophagic flux might be either impaired fusion between autophagosomes and lysosomes or lysosomal dysfunction. To determine the cause(s) for the blockage of autophagic flux, corneal fibroblasts were treated with bafilomycin A<sub>1</sub> and compared with untreated corneal fibroblasts. Bafilomycin A<sub>1</sub> is an autophagy inhibitor that inhibits fusion between autophagosomes and lysosomes by blocking the vacuolar-type H<sup>+</sup>-translocating ATPase. As shown in Figure 4I–K, LC3-II, SQSTM1 levels were gradually enhanced in WT corneal fibroblasts treated with bafilomycin A<sub>1</sub> ranging from 0.02 to 0.04  $\mu$ M. However, the LC3-II and SQSTM1 protein levels decreased in fibroblasts treated with 0.06  $\mu$ M bafilomycin A<sub>1</sub> compared to 0.04  $\mu$ M bafilomycin A<sub>1</sub>. Based on the above data, 0.04  $\mu$ M bafilomycin A<sub>1</sub> was chosen for subsequent experiments. The levels of both LC3-II and SQSTM1 were enhanced in WT and MT corneal fibroblasts treated with bafilomycin A<sub>1</sub> compared with untreated WT and MT corneal fibroblasts. Notably, the increased amplitude of protein levels in MT corneal fibroblasts was less than that in WT corneal fibroblasts (Figure 4L,H). In addition, the lysosomes in MT corneal fibroblasts were enlarged as evidenced by LAMP2-positive

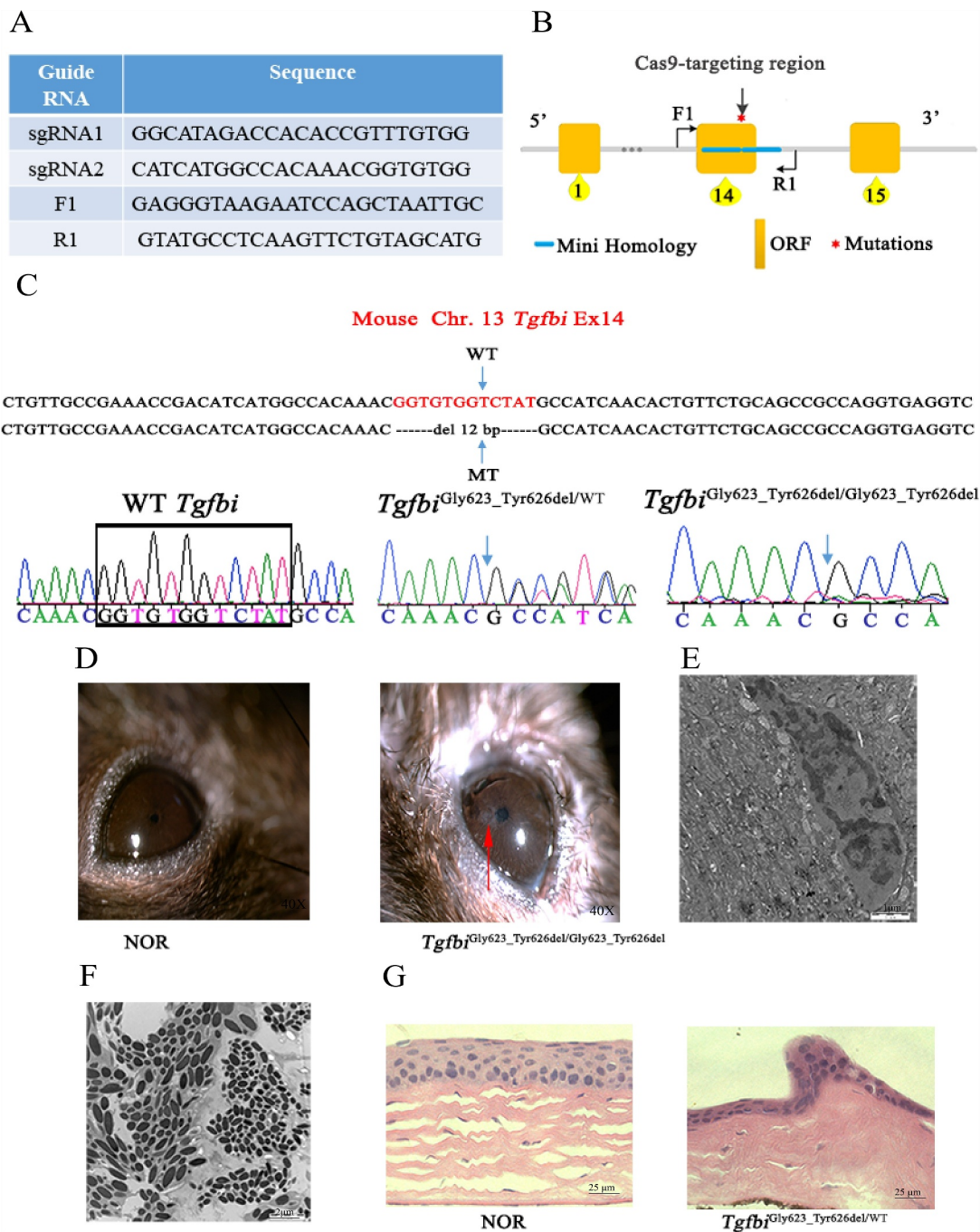


**Figure 3.** SgRNA/Cas9-mediated *Tgfb1*-p.Gly623\_Tyr626del mouse model of TBCD. (A) shows sgRNA sequence and the associated upstream and downstream primers. (B) Schematic representations of targeting strategy for the generation of *Tgfb1*-p.Gly623\_Tyr626del mouse model of TBCD using the CRISPR/Cas9 system. (C) Representative sequencing results of *Tgfb1*-p.Gly623\_Tyr626del homozygous and heterozygous mutant mice in *Tgfb1*. (D) Anterior segment picture of wild-type mice at 42 weeks with no corneal opacities. Corneal opacity is observed in the center of the cornea in a homozygous mouse at 42 weeks of age. Red arrow represents corneal opacity. (E–F) shows TEM images of *Tgfb1*-p.Gly623\_Tyr626del mouse corneal tissue. The results reveal electron-dense deposits and vacuole formation in mouse corneas. (G) HE staining of WT *Tgfb1* and *Tgfb1*<sup>Gly623\_Tyr626del/WT</sup> mice corneal tissues. Intraepithelial extensions of basal lamina material of *Tgfb1*<sup>Gly623\_Tyr626del/WT</sup> mice could be obviously observed (scale bars: 40X in D; 1  $\mu$ m in E; 2  $\mu$ m in F; 25  $\mu$ m in G).

vesicles. Colocalization of LC3 puncta with LAMP2 was higher in MT compared with WT corneal fibroblasts (Figure 4N). The quantification analysis is shown in Fig. S3A. Taken together, these findings indicate that, in TBCD, autophagosome could fuse with lysosome and the blockage of autophagic flux might probably be derived from the dysfunction of lysosomes.

#### Lysosomal dysfunction in TBCD corneal fibroblasts

Maintaining a stable acidic pH is essential for optimal function of lysosomes. The pH-sensitive indexes of lysosomal function can be affected by lysosomotropic dyes, such as LysoTracker Green [28]. To gain further insight into

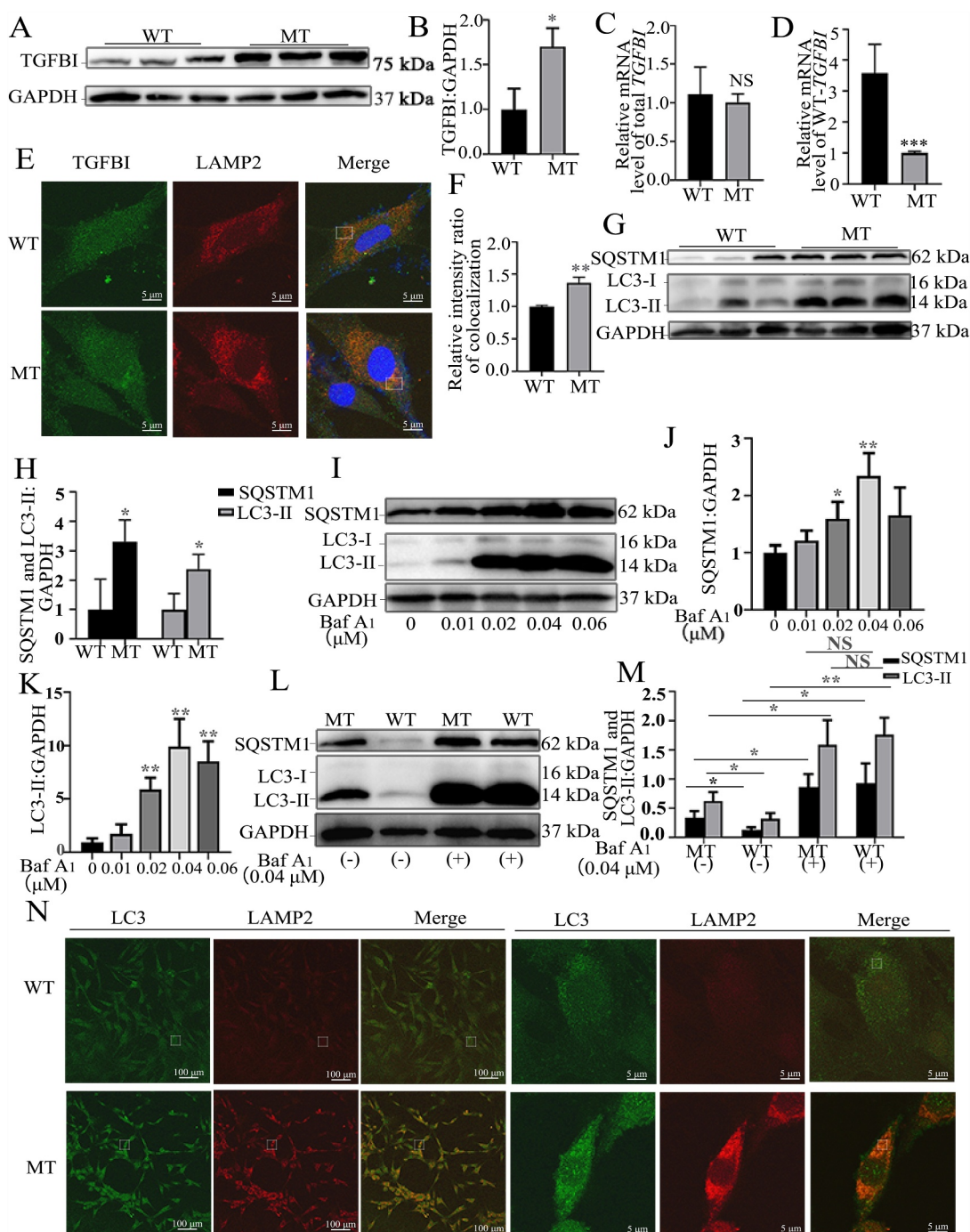


**Figure 4.** TGFBI metabolism and autophagy impairment in TBCD corneal fibroblasts. (A) TGFBI were analyzed by western blotting in WT and MT. The TGFBI:GAPDH data are shown in (B). \*  $p < 0.05$ ;  $n = 3$  for each group; (C-D) mRNA levels of total *TGFBI* and WT-*TGFBI* in WT and MT were analyzed. The ratios of the mRNA level of total *TGFBI* and WT-*TGFBI* to that of *GAPDH* mRNA are shown. NS = no significance; \*\*\* $p < 0.001$ ;  $n = 3$  for each group; (E) WT and MT corneal fibroblasts were subjected to immunostaining for TGFBI (green), LAMP2 (red), and DAPI (blue) followed by confocal microscopy. (F) The quantification of the colocalization ratio of TGFBI and LAMP2 in (E). \*\*  $p < 0.01$ ;  $n = 3$  for each group. (G) The expression of LC3-II and SQSTM1 were analyzed in WT (from three different WT corneal fibroblasts line) and MT corneal fibroblasts. (H) shows significant differences in MT compared with WT corneal fibroblasts of LC3-II and SQSTM1 levels. \*  $p < 0.05$ ,  $n = 3$  for each group; (I) Western blotting analysis of LC3-II and SQSTM1 levels in WT corneal fibroblasts treated with bafilomycin A<sub>1</sub> (0–0.06  $\mu\text{M}$ ). (J-K) Western blotting was quantified from WT corneal fibroblasts after normalization to GAPDH. \*  $p < 0.05$ ; \*\*  $p < 0.01$ ,  $n = 3$  for each group; (L) LC3-II and SQSTM1 levels were assessed by western blotting treated with or without bafilomycin A<sub>1</sub> (0.04  $\mu\text{M}$ ) in WT and MT. Quantification of LC3-II and SQSTM1 levels presented in (M) after normalization to GAPDH protein signals. \*  $p < 0.05$ ; \*\*  $p < 0.01$ ; NS = no significance,  $n = 3$  for each group. (N) WT and MT corneal fibroblasts were subjected to immunostaining for LC3 (green) and LAMP2 (red) followed by confocal microscopy. The enlarged photographs from the left three boxed areas are shown in the right three panels. The quantification of the colocalization ratio in the above groups was shown in Fig. S3A. Error bars indicate standard deviation (SD). (scale bars: WT or MT 5  $\mu\text{m}$  in E; WT or MT 100  $\mu\text{m}$ , 5  $\mu\text{m}$  in N).

lysosomal functions, we performed FC (flow cytometry) and found a loss of the LysoTracker signal in MT corneal fibroblasts compared with the LysoTracker signal observed in WT (Figure 5A,B). As mentioned before, lysosomes function

mainly through numerous proteolytic enzymes contained in the cell organelle. Therefore, in order to find the key abnormal proteins in lysosomes, proteomic analysis was conducted to determine the protein expression profiles in WT and MT

corneal fibroblasts. The proteome profiles of WT and MT corneal fibroblasts were compared. A total of 6,228 proteins were identified, among which 5,521 proteins contained quantitative information. These data revealed a dramatic shift in the protein differential expression, reflected by 129 upregulated proteins and 89 significantly downregulated proteins

between WT and MT corneal fibroblasts with a cutoff for the fold-change > 1.5 and significance P values of < 0.05 (Figure 5C). Figure 5D,E show the ratio of expression of a class of differentially expressed proteins that caught our attention; the specific contents are as follows: TGFBI (2.318 fold-change,  $p = 0.00996$ ), CTSD (-0.666 fold-change,

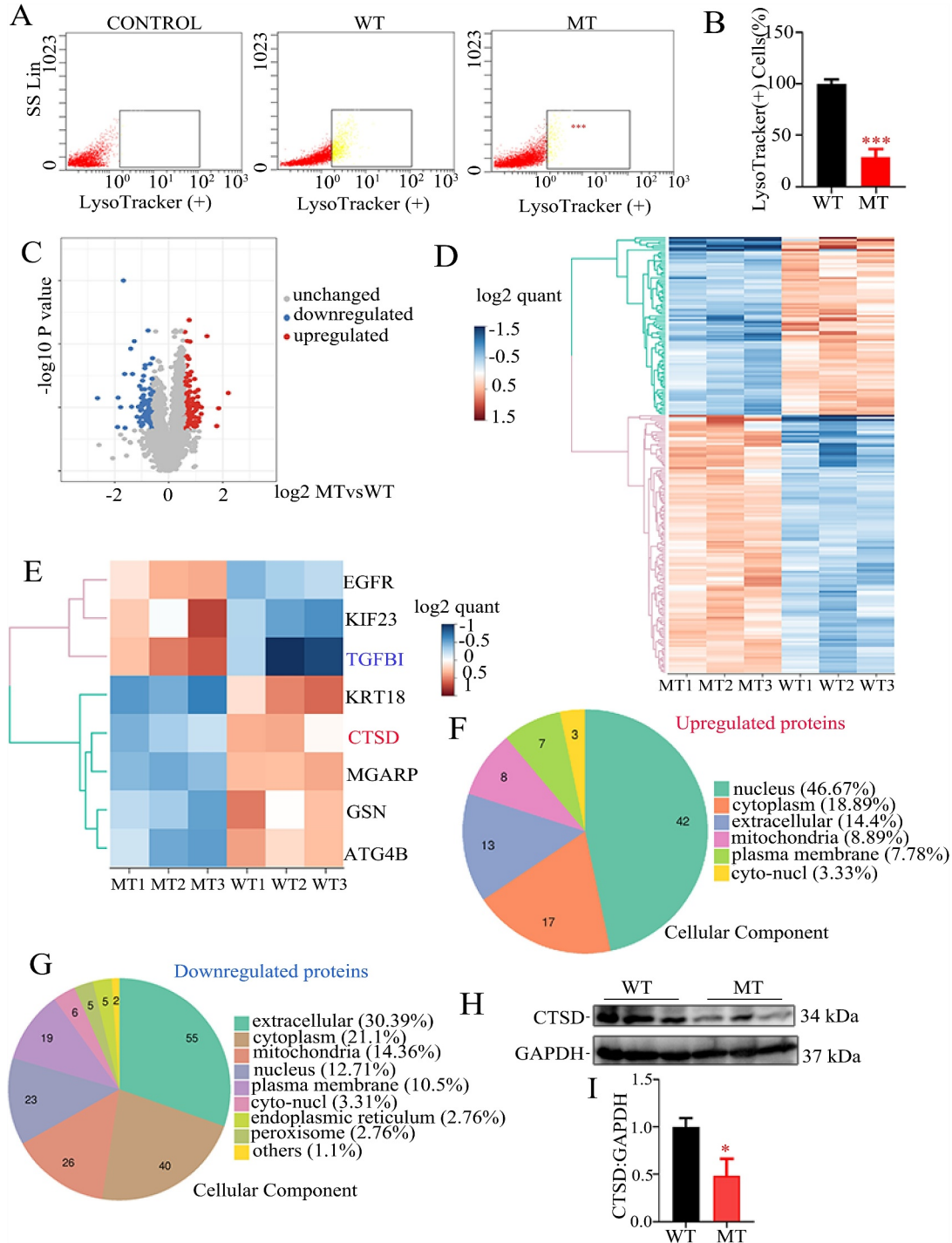


**Figure 5.** Lysosomal dysfunction in TBCD corneal fibroblasts. (A–B) A tendency toward lower expression of LysoTracker Green (+) cells was shown in lysosome function analysis by FC in MT corneal fibroblasts compared to WT. \*\*\*  $p < 0.001$ ,  $n = 3$  for each group; (C) The quantitative protein expression in MT corneal fibroblasts was shown in the volcano plot of statistical significance against log<sub>2</sub>-fold change and shaded upregulated proteins in red as well as downregulated proteins in blue compared to WT. (D–E) Heatmap of the differentially expressed proteins in MT corneal fibroblasts compared with WT. Heatmap of the vital differentially expressed proteins in MT corneal fibroblasts versus WT. (F–G) show the subcellular distribution of the differentially expressed proteins. (H–I) The protein levels of CTSD in WT and MT corneal fibroblasts were verified by western blotting. \*  $p < 0.05$ ;  $n = 3$  for each group. Error bars indicate SD.



$p = 0.0126$ ), and ATG4B ( $-0.620$  fold-change,  $p = 0.0618$ ). Investigation of the subcellular distribution of differentially expressed proteins showed that the largest proportion of the upregulated differentially expressed proteins identified were annotated as nucleus (46.67%), followed by cytoplasm (18.89%), extracellular (14.4%), and mitochondrion (8.89%). Among the downregulated differentially expressed proteins, extracellular (30.39%) accounted for the largest proportion, followed by cytoplasm (21.1%), mitochondrion (14.36%), and nucleus (12.71%) (Figure 5F,G). These proteomics data indicate that the expression of CTSD is significantly reduced. Consistent with the proteomics data, western blotting further confirmed the meaningful decline of CTSD in MT corneal fibroblasts in contrast to WT (Figure 5H,I). Therefore, we speculate that the blockage of autophagic flux and mutant TGFBI accumulation might be a result of lysosomal alkalization and loss of CTSD.

### Impaired TFEB-mediated dysfunction of the lysosome and autophagy process in TBCD corneal fibroblasts and potential reversal of this dysfunction with torin 1

TFEB is regarded as an upstream regulator of the lysosomal system and autophagy biogenesis. Thus, we investigated whether the dysfunction of lysosomes in TBCD corneal fibroblasts could be due to impaired TFEB function. Strikingly, a distinct decrease in total TFEB was observed in MT compared with WT corneal fibroblasts (Figure 6A,B). Following dephosphorylation, TFEB translocated to the nucleus and was activated. Next, the cytoplasmic and nuclear TFEB protein levels were measured in MT and WT corneal fibroblasts. As expected, cytoplasmic and nuclear TFEB protein levels were markedly lower in MT than in WT corneal fibroblasts (Figure 6C–E). Confocal microscope analysis revealed that, under the normal state, the quantify of activated TFEB in

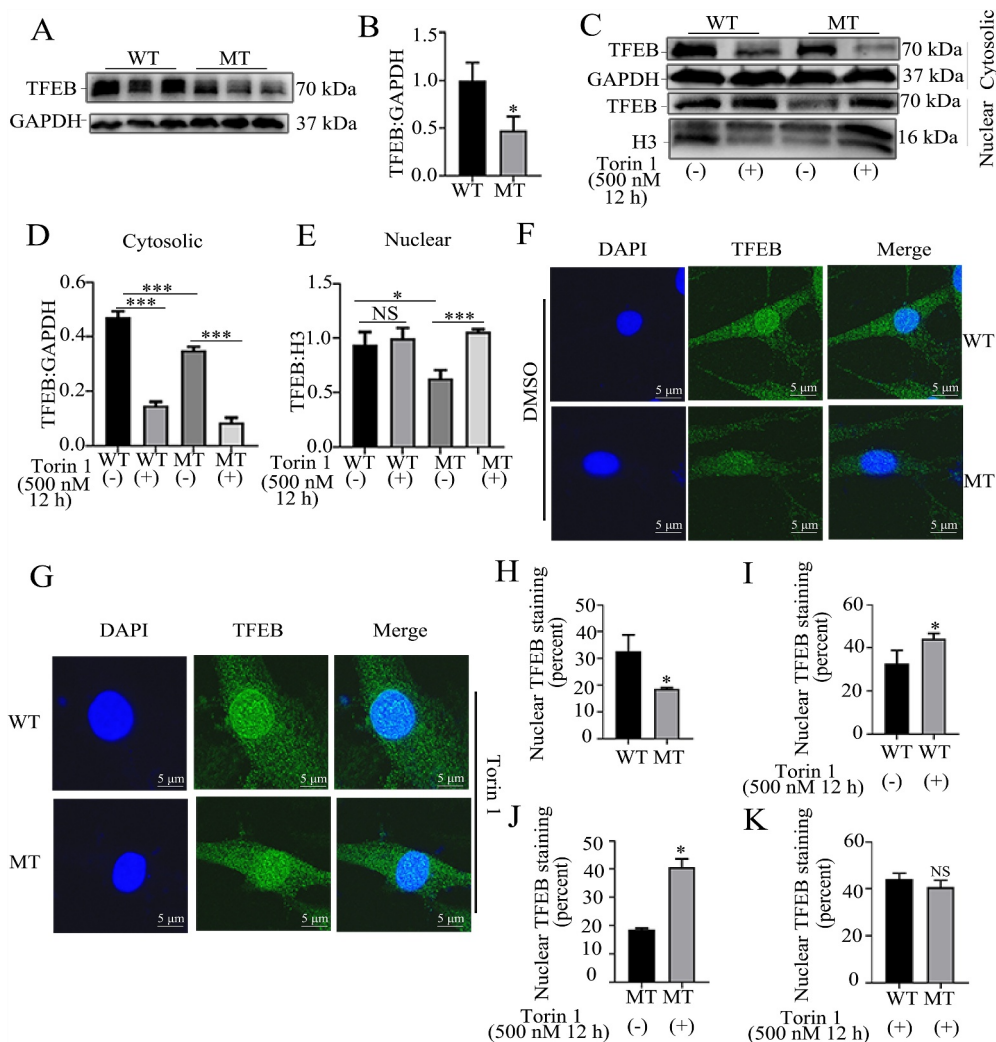


**Figure 6.** Total and activation of TFEB were reduced in TBCD corneal fibroblasts. (A) Western blotting analysis of total TFEB protein levels in WT and MT. Data were normalized against GAPDH, as shown in (B) \*  $p < 0.05$ ;  $n = 3$  for each group; (C) Decreased cytosolic and nuclear TFEB proteins in MT versus WT and the treatment with torin 1 enhanced the translocation from cytoplasm to nucleus in both WT and MT. (D–E) show data analysis of (C) normalized separately against GAPDH and H3. \*  $p < 0.05$ ; \*\*\*  $p < 0.001$ ; NS = no significance;  $n = 3$  for each group; (F–G) Confocal microscopy analysis of the subcellular distribution of TFEB in WT and MT treated with or without 500 nM torin 1 for 12 h. (H–K) Quantification of the relative TFEB level in the nucleus of WT and MT in (F–G). \*  $p < 0.05$ ; NS = no significance;  $n = 3$  for each group; Error bars indicate SD. (scale bars: WT or MT 5  $\mu\text{m}$  in F and G).

the nucleus was decreased in MT compared with WT corneal fibroblasts (Figure 6F,H).

The activation of TFEB leads to a coordinated upregulation of CLEAR genes, which collectively improves the efficiency of vesicular trafficking and promotes the eventual substrate degradation in the lysosome. We postulated that torin 1, a known MTOR inhibitor, could accelerate the degradation of the accumulated mut-TGFBI in MT corneal fibroblasts via elevating dephosphorylated TFEB to translocate into the nucleus. Our data showed that the expression level of cytoplasmic TFEB protein was dramatically decreased in both WT and MT corneal fibroblasts that had been treated with torin 1 (500 nM, 12 h). Conversely, the expression level of nuclear TFEB protein was enhanced in both WT and MT corneal fibroblasts that had been treated with torin 1 (500 nM, 12 h) (Figure 6C–E). The fluorescent signal showing nuclear-activated TFEB was greater in corneal fibroblasts treated with 500 nM torin 1 than in untreated corneal fibroblasts (Figure 6G). These results indicate that torin 1 can upregulate the activated TFEB to a similar level in the nuclei of both WT

and MT corneal fibroblasts (Figure 6I,J). Furthermore, torin 1 reversed the level of the activated TFEB in the nuclei of MT corneal fibroblasts to the near-normal level of activated TFEB in the nuclei of WT corneal fibroblasts (Figure 6K).

Our findings indicate that torin 1 treatment (500 nM, 12 h) potentially increased dephosphorylated TFEB to translocate into the nucleus and induce the elevation of activated TFEB, thereby augmenting autophagic flux and confirming the upregulated expression of LC3 and CTSD as well as the downregulated expression of SQSTM1 in both WT and MT corneal fibroblasts (Figure 7A–D). Additionally, we found that torin 1 treatment (500 nM) produced a time-dependent decline in levels of mut-TGFBI and SQSTM1 (Figure 7E,F) in MT corneal fibroblasts and that administration of torin 1 (500 nM, 12 h) reversed lysosomal dysfunction (Figure 8A–C) in both WT and MT corneal fibroblasts as shown via confocal microscopic analysis and FC. Confocal microscopic analysis also revealed that torin 1 caused an increase of colocalization puncta of LC3 and LAMP2 not only in WT corneal fibroblasts, but also in MT corneal fibroblasts (Figure 8D). The quantification of the colocalization

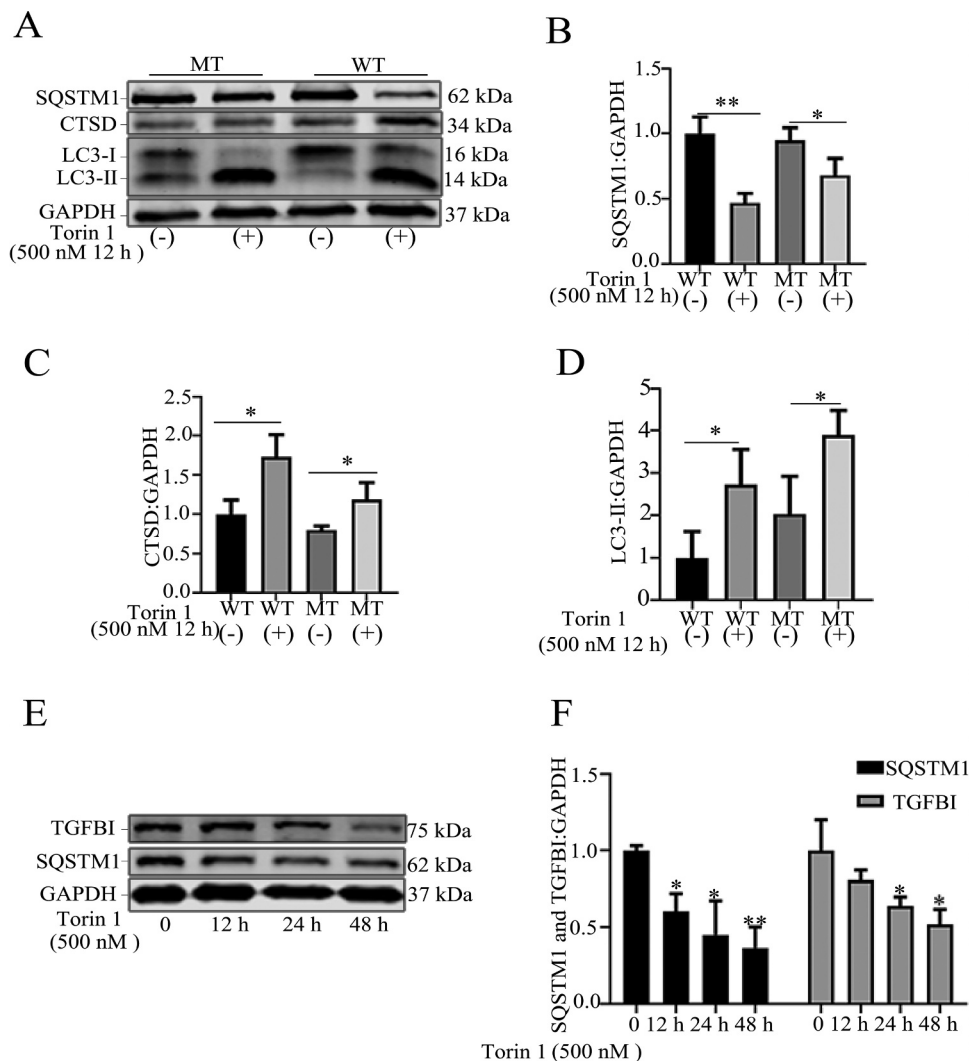


**Figure 7.** Torin 1 enhanced autophagic flux via activating TFEB resulting in the degradation of mut-TGFBI. (A) Torin 1 enhanced autophagic flux marked by decreased SQSTM1 levels and increased LC3-II and CTSD levels in both WT and MT. (B–D) show normalized data in (A) \*  $p < 0.05$ , \*\*  $p < 0.01$ ,  $n = 3$  for each group; (E) The SQSTM1 and mut-TGFBI were degraded gradually over time in MT, and data analysis is shown in (F) \*  $p < 0.05$ , \*\*  $p < 0.01$ ,  $n = 3$  for each group. Error bars indicate SD.

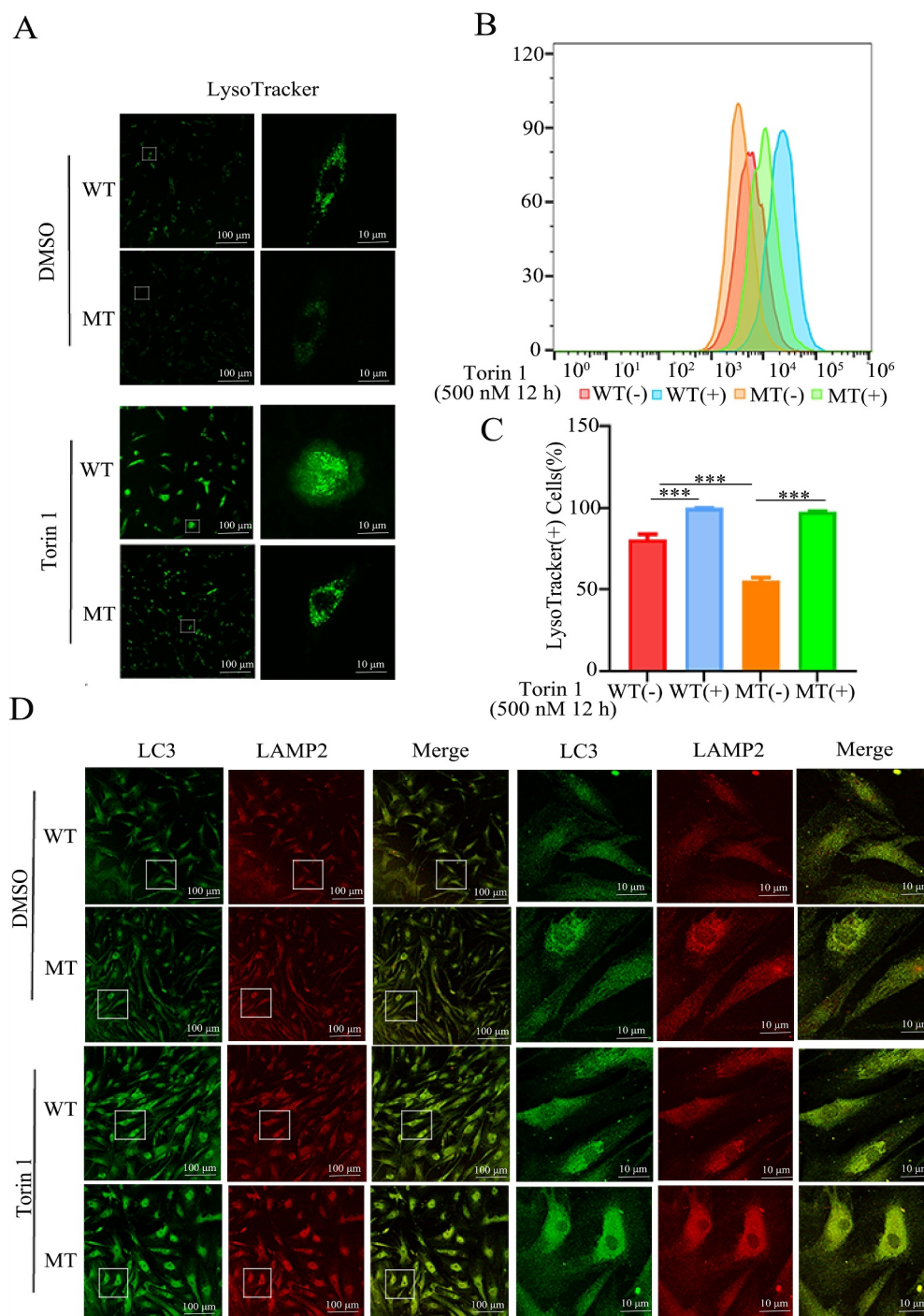


**Figure 8.** Torin 1 reversed lysosomal dysfunction and enhanced autophagic flux. (A) Confocal microscopy analysis shows lysosome function was reversed in both WT and MT after treatment with 500 nM torin 1 for 12 h using LysoTracker Green. (B-C) This result was also confirmed by FC analysis. (D) MT and WT corneal fibroblasts were subjected to 500 nM torin 1 for 12 h then immunostained for LAMP2 (red) and LC3 (green) followed by confocal microscopy. The enlarged photographs from the left boxed areas are shown in the right three panels. The quantification of the colocalization ratio in the above groups was shown in Figure S3B. Error bars indicate SD. (scale bars: WT or MT 100  $\mu$ m, 10  $\mu$ m, respectively, in A; DMSO or torin 1: WT or MT 100  $\mu$ m, 10  $\mu$ m, respectively, in D).

puncta indicated that torin 1 might promote autophagosome-lysosome fusion (Fig. S3B). These data illustrate that, in TBCD corneal fibroblasts, there is a downward trend in total and cytoplasmic, as well as nucleic TFEB expression and that torin 1 can reverse nucleic TFEB expression and subsequently enhance the autophagic flux, as well as ameliorate lysosomal dysfunction, leading to a decrease in aggregated mut-TGFBI.

### Overexpression of mutant TGFBI impaired the autophagy-lysosome process in HEK 293 cells

To investigate whether TGFBI gene mutations may cause TGFBI deposition and impair the autophagy-lysosome process in other cell lines, human full-length WT-TGFBI (hereafter, HEK 293 pCAGGS-TGFBI-WT), mut-TGFBI

(hereafter, HEK 293 pCAGGS-*TGFBI*-MT), and only a pCAGGS (hereafter, HEK 293 pCAGGS) were transferred into HEK 293 cells via pCAGGS plasmid. As expected, there was only slight expression of *TGFBI* in HEK 293 pCAGGS; however, the level of *TGFBI* in HEK 293 pCAGGS-*TGFBI*-MT was obviously increased compared with HEK 293 pCAGGS-*TGFBI*-WT after transfection for 72 h (Figure 9A,B). The above results indicate that the accumulated *TGFBI* observed in HEK 293 pCAGGS-*TGFBI*-MT was caused by the in-frame mutation of the *TGFBI* gene. Furthermore, the level of LC3-II in HEK 293

pCAGGS-*TGFBI*-MT also tended to be higher (Figure 9A, C). A significant increase in the SQSTM1 level was observed in HEK 293 pCAGGS-*TGFBI*-MT compared with HEK 293 pCAGGS and HEK 293 pCAGGS-*TGFBI*-WT (Figure 9A,D). Similar changes were also observed via immunofluorescence analysis. The fluorescence intensity of *TGFBI* in HEK 293 pCAGGS-*TGFBI*-MT was higher compared with HEK 293 pCAGGS and HEK 293 pCAGGS-*TGFBI*-WT (Figure 9E,F). Analogous to human TBCD corneal fibroblasts, after transfection for 72 h, HEK 293 pCAGGS-*TGFBI*-MT exhibited a LysoTracker

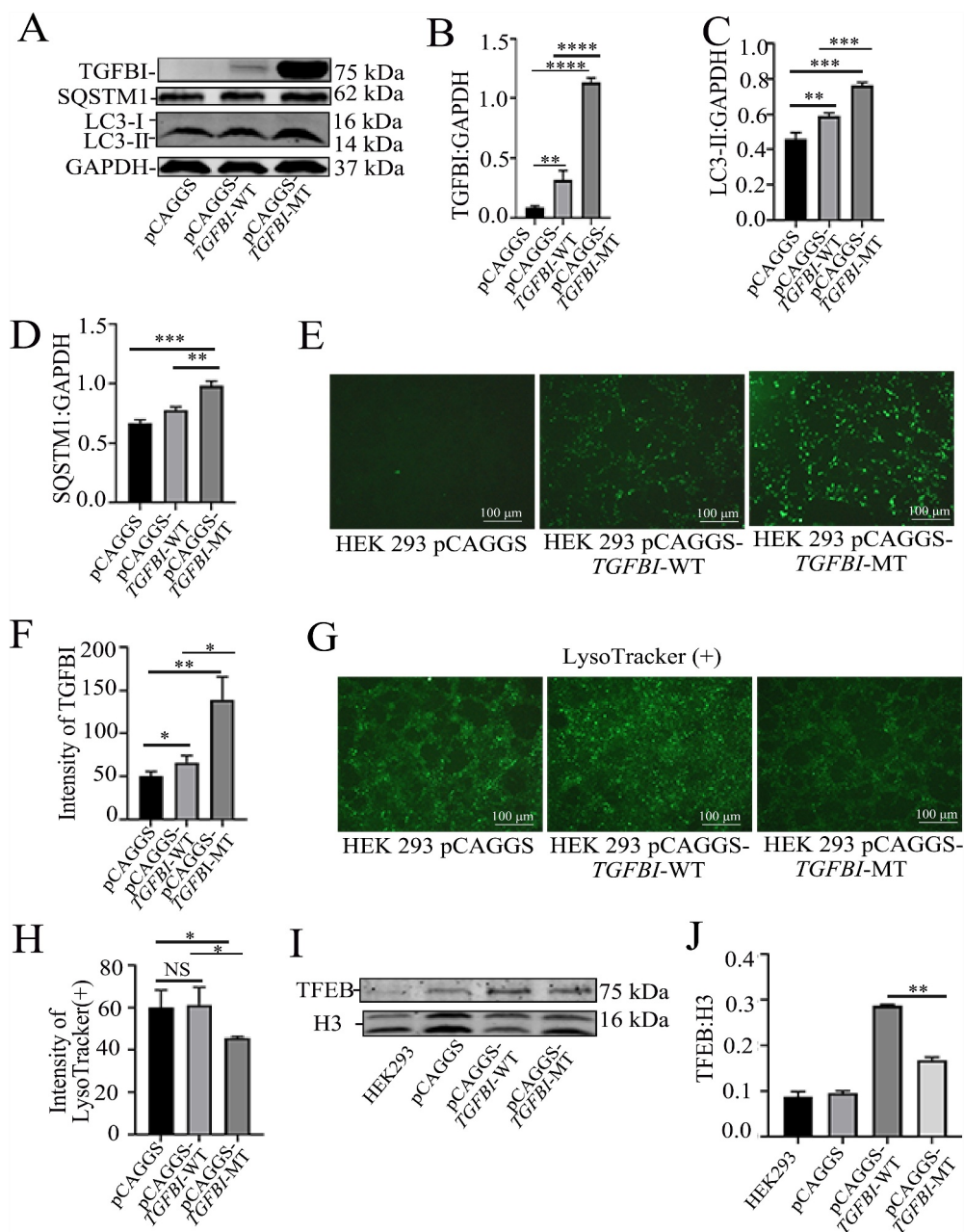


**Figure 9.** Western blotting and immunofluorescence analysis in transfected HEK 293 cell line. (A) Western blotting analysis of *TGFBI*, SQSTM1, LC3-II in HEK 293 pCAGGS, HEK 293 pCAGGS-*TGFBI*-WT and HEK 293 pCAGGS-*TGFBI*-MT transfected for 72 h. (B–D) show normalized data in (A) \*\*  $p < 0.01$ , \*\*\*  $p < 0.001$ , \*\*\*\*  $p < 0.0001$ ,  $n = 3$  for each group; (E) showed the immunofluorescence analysis of *TGFBI* in HEK 293 pCAGGS, HEK 293 pCAGGS-*TGFBI*-WT and HEK 293 pCAGGS-*TGFBI*-MT transfected for 72 h and the quantification was shown in (F) \*  $p < 0.05$ ; \*\*  $p < 0.01$ ,  $n = 3$  for each group. (G) showed the immunofluorescence analysis of LysoTracker (+) fluorescence in HEK 293 pCAGGS, HEK 293 pCAGGS-*TGFBI*-WT and HEK 293 pCAGGS-*TGFBI*-MT and the quantification was shown in (H). \*  $p < 0.05$ ; NS = no significance;  $n = 3$  for each group. (I) Western blotting analysis of nucleus TFEB in HEK 293 pCAGGS, HEK 293 pCAGGS-*TGFBI*-WT and HEK 293 pCAGGS-*TGFBI*-MT transfected for 72 h. (J) The normalized data in (I) \*\*  $p < 0.01$ ,  $n = 3$  for each group; Error bars indicate SD. (scale bars: 100  $\mu\text{m}$  in E and G).

fluorescence signal deficiency compared with HEK 293 pCAGGS-*TGFBI*-WT, as well as HEK 293 pCAGGS-*TGFBI*-MT (Figure 9G,H). These results suggest that the autophagy flux was obstructed and that there was lysosome dysfunction in HEK 293 pCAGGS-*TGFBI*-MT cell line. Noticeably, a significant decrease in activated TFEB was manifested in the nuclei of HEK 293 pCAGGS-*TGFBI*-MT compared with HEK 293 pCAGGS-*TGFBI*-WT after transfection for 72 h (Figure 9I,J). However, there was no difference in total TFEB or activated TFEB between the nuclei of HEK 293 pCAGGS-*TGFBI*-MT and HEK 293 pCAGGS-*TGFBI*-WT after transfection for 48 h, probably due to insufficient transfection time (Fig. S4A-D). Taken together, the above data further confirm that the accumulated mut-*TGFBI* was due to the c.1868–1879 del mutation of *TGFBI* and the impaired autophagy and lysosomal dysfunction, as well as the downregulated dephosphorylated TFEB in the HEK 293 pCAGGS-*TGFBI*-MT cell line.

In conclusion, a schematic diagram summarizes the probable pathogenic molecular mechanism of TBCD featured by blockage of autophagic flux resulting from alkalization of lysosomes and the deficiency of CTSD (Figure 10).

## Discussion

The current study presents the first report of a TBCD pedigree associated with a novel in-frame mutation in the *TGFBI* gene; a heterozygous c.1868–1879del mutation on 5q31 chromosome in exon 14. We found that, in TBCD corneal fibroblasts, the obstructed autophagy flux directly impacts mut-*TGFBI* accumulation and lysosomal alkalization and that the deficiency of CTSD might be responsible for this blockade. Furthermore, it was found that TFEB plays a critical role in the modulation of autophagy and lysosomal biological processes and that a decrease in TFEB might be the main cause of lysosomal dysfunction. More importantly, torin 1 enhanced TFEB levels contributing to profound impacts on the

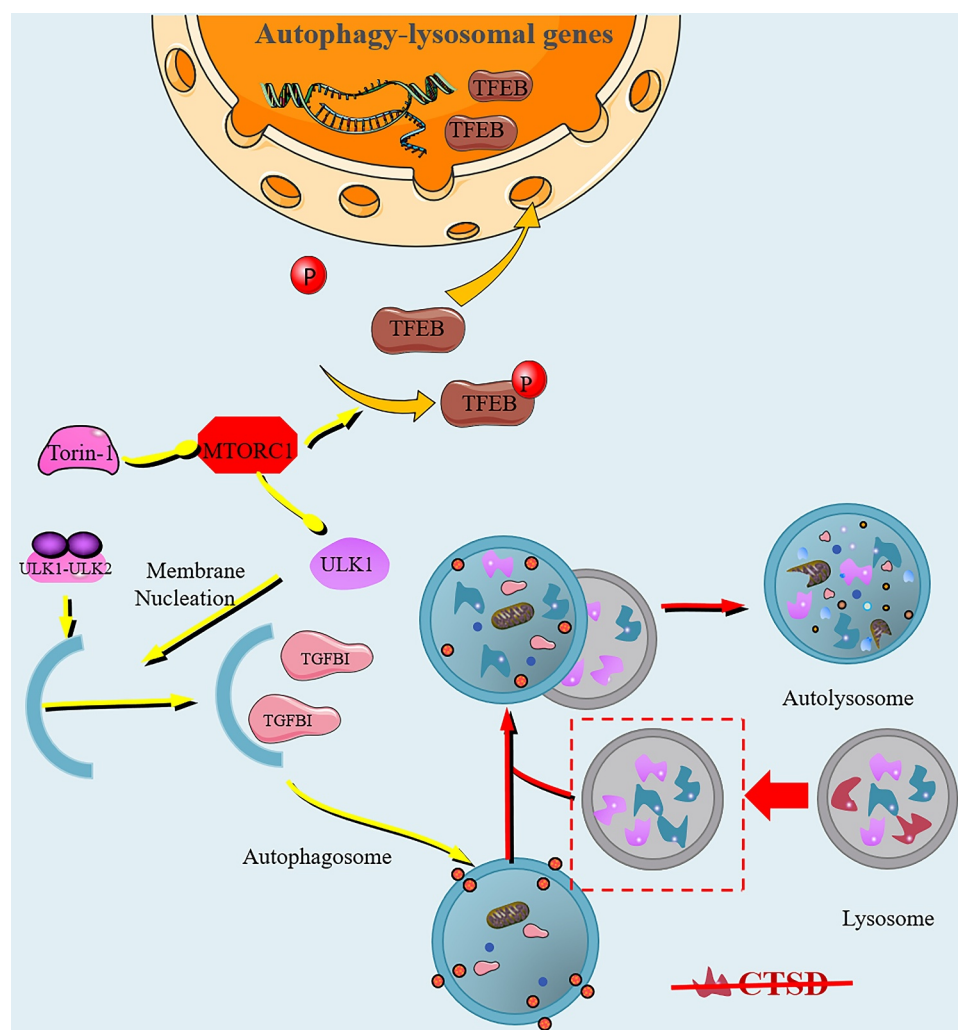


**Figure 10.** A proposed model of TFEB interacts with the MTORC1 complex and the dysfunction of lysosome in autophagy pathways in TBCD. At the initial stage of autophagy, the phagophore surrounds mut-*TGFBI* and forms a double-membrane autophagosome. After that, the autophagosome fuses with lysosomes and the sequestered contents are degraded by lysosomal hydrolases. However, decreased TFEB in the nucleus directly leads to decreased lysosomal biogenesis, resulting in the reduction in the main lysosomal hydrolase CTSD and insufficient autophagy. Pharmacological inhibition of MTORC1 may promote TFEB nuclear translocation and related lysosomal biogenesis. We hypothesize that, in TBCD, torin 1 might increase TFEB-mediated lysosomal biogenesis in such a way as to rescue the insufficient autophagy.

degradation of mut-TGFBI in TBCD, suggesting that torin 1 might be a promising therapeutic target for TBCD.

TGFBI is initially translated on ribosomes bound to endoplasmic reticulum, and then translocated to the endoplasmic reticulum where it undergoes a series of processes to attain full biological activity. The Golgi apparatus sorts the proteins and secretes them, in the form of secretory vesicles, to intracellular functional sites [29]. Some aggregates of mut-TGFBI are likely wrapped and form large multivesicular bodies that are trafficked to the plasma membrane, where, upon fusion with the plasma membrane, they release their contents into the extracellular space via the exosome pathways [30]. Mut-TGFBI in ECM is hydrolyzed by a series of proteolytic enzymes, such as MMPs, aminopeptidase [31], and HTRA1. Some *TGFBI* gene-related corneal dystrophies are caused by abnormalities of the extracellular proteolytic process. The main driving force of the LCD disease may be the removal of the degradation products of TGFBI by HTRA1, as this process can release peptides that are prone to amyloid fibrillation, leading to the deposition of amyloid in the cornea [20]. We speculated that there were the aggregations of mut-TGFBI in ECM in TBCD. The reason for this accumulation is likely similar to LCD, since elevated ECM hydrolyzed protein MMP3 was found by proteomic analysis (Fig. S5). The other two possible intracellular main degradation pathways of mut-TGFBI are considered to be the ubiquitin/proteasome and autophagy pathways. Previous reports have provided a compelling rationale that mut-TGFBI in corneal fibroblasts are localized to Golgi, and later appear in lysosomes, and are mainly degraded by autophagy rather than through the ubiquitin/proteasome pathway [26]. Post-translational modifications of ubiquitins in our study confirmed that there were no significant ubiquitin differences in TBCD. Conversely, accumulations of mut-TGFBI were encapsulated to form autophagosomes. Nonetheless, lysosomal alkalization and decreased CTSD resulted in an insufficient number of lysosomes fusing with autophagosomes, thus causing autophagic flux blockage and mut-TGFBI aggregation.

TFEB, a key autophagy and lysosome signal regulator factor, has been associated with lysosomal biogenesis and autophagy via affecting lysosomal hydrolases, lysosomal membrane proteins, and proteins [9]. The activity of TFEB is regulated by MTOR-mediated phosphorylation, and phosphorylated TFEB is retained in the cytoplasm; whereas dephosphorylated TFEB translocates to the nucleus to induce the transcription of target genes [32]. A series of kinases that phosphorylate TFEB has been identified; namely MTORC1, MAPK1/ERK2, PRKCB (protein kinase C beta) and AKT [33,34]. TGFBI can trigger phosphorylation and activation of AKT and MAPK/ERK [35], which raises the speculation that a reduction in activated forms of TFEB in TBCD corneal fibroblasts might be due to the activation of AKT and MAPK/ERK resulting from the accumulated TGFBI. Importantly, data in the current study shed light on the fact that torin 1, a specific inhibitor of MTOR, also known as an activator of TFEB, probably decreased the accumulated mut-TGFBI in TBCD corneal fibroblasts resulting in enhanced autophagic flux and reversed lysosomal function, which was related to the increased dephosphorylated TFEB to some degree. Nevertheless, the protein kinase, torin 1 inhibited both MTORC1 and MTORC2, and also affected other pathways, especially the AKT-

mediated survival signaling pathway, via promoting growth factor-mediated cell survival and blocking apoptosis. Therefore, the safety and feasibility of using torin 1 as a potential therapeutic for TBCD needs further exploration. The plant-derived polyphenolic compound, Quercetin, enhances the TFEB-mediated lysosomal-autophagy pathway in RPE cells, effectively inhibiting MTORC1 without affecting AKT phosphorylation [36]. Recently, trehalose was found to induce TFEB nuclear translocation and promote autophagic flux via the inhibition of AKT against inflammation and might be beneficial in primary HCECs exposed to hyperosmotic in dry eye [37]. Whether Quercetin or trehalose can also be used in the treatment of TBCD needs to be further examined. Although limited research has focused on TFEB-associated therapy in TBCD, the possibility that it may be of benefit in TBCD patients has been extensively accepted. There are other therapeutic possibilities for enzyme replacement therapy for recombinant CTSD. Studies have shown that dosing of rhCTSD in the murine CTSD/CLN10 model leads to a correction of lysosomal hypertrophy, storage accumulation, and impaired autophagic flux in the viscera and the central nervous system [6]. Therefore, it is possible that the blockage of autophagic flux in TBCD might be alleviated to some extent with rhCTSD treatment. However, rhCTSD is a type of pro-CTSD protein, and needs to undergo proteolytic processing and maturation within a specific pH. Alkaline pH in TBCD might not provide the optimum pH environment for maturation and may lead to inactivation of rhCTSD. Therefore, initially modifying the raised pH in TBCD should be considered; otherwise, recombinant CTSD might not be activated and will have the same fate as endogenous CTSD. Identifying the upstream regular signals of CTSD might also be helpful for TBCD therapy. Studies have demonstrated that CTSL is able to degrade CTSD, which then cleaves to CASP3 [38]. CTSD might act as a key player in the switch from apoptosis to autophagy. However, whether inhibition of CTSL expression by a Z-FY-CHO inhibitor could specifically enhance the level of CTSD in TBCD to promote the switch from apoptosis to autophagy has not yet been elucidated.

Studies have described that establishment of a transgenic mouse model with a mutated *Tgfb1* gene R124 H and R124 C would be helpful for studying the pathogenesis and treatment of *TGFBI*-linked corneal dystrophies. A granular corneal dystrophy type 2 mouse model was established via R124H mutation of *Tgfb1* and cross-sectional studies in this model revealed that genotype and age were associated with the incidence of corneal opacity [39]. The *Tgfb1*<sup>R124C</sup> mutant mouse model was established via CRISPR/Cas9 and is characterized by corneal opacity owing to the accumulation of mut-TGFBI and delayed epithelial wound healing similar to that observed in human patients with R124C LCD; though this model might not be a reliable as a LCD1 model due to the lack of amyloid deposition [40]. Currently, to the best of our knowledge, no animal models of human TBCD are available. In our study, by mimicking *TGFBI* gene mutation in humans, we successfully generated a *Tgfb1*-p.Gly623\_Tyr626del mouse model of TBCD carrying *Tgfb1* gene c.1867–1878 GTGTGGTCTATG del using CRISPR/Cas9 technology. The mice developed corneal opacities at 42 weeks of age, and these changes were consistent with what is observed in human TBCD. Features of human TBCD, including thinness of the corneal epithelium and vacuolization changes of the corneal stroma were reproduced in this

model. Collectively, our *in vitro* studies suggest that Torin 1 can degrade the pathological deposits of mut-TGFBI and we speculated that it might also be applied therapeutically in the treatment of *TGFBI* mutation-related corneal dystrophies. The effective ingredients of this drug were extracted and administered to *Tgfb1*-p.Gly623\_Tyr626del mice via eye drops, which probably enhanced the lysosomal-autophagic flux and the degradation of mut-TGFBI. This model provides a vital avenue for future research and may lead to possible new treatment options for patients suffering from TBCD.

Our study demonstrated that the heterozygous c.1868–1879del mutation in TBCD corneal fibroblasts resulted in accumulation of TGFBI, accompanied by autophagic flux blockage and lysosomal dysfunction. In addition, our experiments revealed that TGFBI may be predominantly degraded via an intracellular lysosome-dependent autophagy pathway in TBCD corneal fibroblasts. Nevertheless, further research into whether the intracellular lysosome-dependent autophagy pathway is responsible for the degradation of TGFBI in various types of *TGFBI*-linked corneal dystrophies is required.

## Conclusion

In summary, this study not only uncovers a novel mutation of the *TGFBI* gene (c.1868–1879del heterozygous in-frame mutation) in TBCD patients that had not yet been reported, but also identifies a possible mechanism, lysosomal alkalization and dysfunction that obstructs autophagy flux, for accumulated mut-TGFBI in TBCD corneal fibroblasts. In future work, the feasibility of using torin 1 for the treatment of TBCD will be investigated in the *Tgfb1*-p.Gly623\_Tyr626del TBCD mouse model and other possible therapeutics for TBCD will be explored.

## Materials and methods

### Patients and clinical examinations

Seven patients from the TBCD pedigree received clinical diagnoses by three doctors using slit-lamp biomicroscopy at the First Affiliated Hospital of Harbin Medical University. Our control group was not age- or sex-matched with the experimental group, and no ophthalmic examination was performed on these individuals. Clinical examination consisted of visual acuity, slit-lamp biomicroscopy with photography, endothelial cell measurements, and AS-OCT. Anterior segment imaging was performed by one observer. Twenty normal relatives from this pedigree received all the above ophthalmic examinations (Table S1). The study was conducted in accordance with the Declaration of Helsinki and was approved by the Ethics Committee of Harbin Medical University. All patients signed informed consent before any study procedure.

### Reagents and antibodies

The following reagents and antibodies were used in this investigation: Dulbecco's Modified Eagle Media: Nutrient

Mixture F-12 (Hyclone, SH30023.01); Fetal bovine serum (ExCell Bio, FND500); ubiquitin (Jingjie PTM BioLab, PTM-1107); TGFBI (Abcam, ab170874); SQSTM1/p62 (Becton, Dickinson and Company, 610,833); CTSD (Calbiochem, IM16); LC3 (Cell Signaling Technology, 3868); LAMP2 (Abcam, ab25631); TFEB (Cell Signaling Technology, 4240); TFEB (Abcam, ab270604); GAPDH (Protein Tech, 10,494-1-AP); HRP-conjugated secondary antibody (Zsbio, ZB-2301); Donkey anti-Rabbit IgG (H + L) highly cross-adsorbed secondary antibody (Invitrogen, A32808); Donkey anti-Mouse IgG (H + L) Highly Cross-Adsorbed Secondary Antibody (Invitrogen, A32789); ECL developer (Beyotime, P0018AS); Bafilomycin A<sub>1</sub> (Sigma, B1793); Torin 1 (Cell Signaling Technology, 14,379); LysoTracker Green DND-26 (Cell Signaling Technology, 8783).

### TGFBI analysis

DNA extraction kit (DNeasy Blood and Tissue Kit; QIAGEN, 69,504) was used for the separation of genomic DNA from peripheral leukocytes of 24 members (7 affected and 17 unaffected). To amplify the region of the open reading frame of *TGFBI*, we selected 14 pairs of primers. The specific conditions were as follows: first, a mixture of genomic DNA (100 ng), 25  $\mu$ L of Phanta max buffer, deoxynucleotide triphosphates mix, and Phanta Max Super-Fidelity DNA polymerase (Vazyme Biotech Co., P505-d1) were made to the final reaction mixture 50  $\mu$ L. To amplify the products, the following conditions were performed: 5 min of denaturation at 95°C followed by 35 cycles of denaturation at 95°C for 15 s, annealing for 15 s at 56°C or at 58°C, extension at 72°C by 30 to 60 s/kb, and a further extension step at 72°C for 5 min. The kit (High Pure PCR Product; Roche, 11,732,668,001) was used to identify the above products with an analysis of agarose gel electrophoresis. Sequences were then tested by an automatic fluorometric DNA sequencer (model 373A; Applied Biosystems, Foster City, CA, USA).

### Isolation and culture of primary WT and MT corneal fibroblasts

TBCD was diagnosed by DNA sequence analysis for *TGFBI* mutations and comprehensive analysis of three doctors from the First Affiliated Hospital of Harbin Medical University according to symptoms, signs, and clinical examinations. WT and MT primary corneal fibroblasts were prepared from healthy corneas from individuals with no visual impairment and patient III 1 after penetrating keratoplasty. The corneal epithelium and endothelium were removed from the corneal tissues and the remainder were slit into small pieces. Corneal tissues were placed on a culture plate and maintained in Dulbecco's Modified Eagle Media: Nutrient Mixture F-12 containing 10% fetal bovine serum, 1000 U/ml penicillin, and 1000  $\mu$ g/ml streptomycin (Gibco, 15,070,063) at 37°C under 95% humidity and 5% CO<sub>2</sub>. Suffered a series of propagation and subculture with trypsin-EDTA (Gibco, 25,200–056), fibroblasts from passages 5 to 8 were used in the succedent experiments.

### Plasmid construction and transduction

The gene of WT- and mut-*TGFBI* amplification from the total RNA of the corneal fibroblasts. Human full-length WT- and mut-*TGFBI* ORF cDNA were cloned into the pCAGGS plasmid (made in our laboratory) by enzyme digestion and ligation. After sequencing identification, the plasmid with target gene was transfected into HEK293 (ATCC, CRL-1573) cells by X-treme GENE 9 DNA transfection reagent (Merck, 6365779001) according to the manufacturer's instructions.

### Histological staining and transmission electron microscopic

Corneal specimens of TBCD and healthy individuals were first fixed in 10% buffered formalin, sectioning of the tissue samples, and then stained hematoxylin and eosin for the analysis by light microscopy examination. Furthermore, tissue masses were immersed in ethanol 100%, rinsed in water, immersed in acetic acid 3%, and subsequently stained in 1% Alcian blue 8GX (Changchun Semerete Technology Co., SM-RT-027) in 3% acetic acid (pH 2.5) for 3 h. By rinsing slides with 3% acetic acid and water, nonspecific stains were removed. After being subsequently oxidized in 1% periodic acid and water, slides were immersed in Schiff's reagent, and then rinsed in water 0.5% sodium metabisulphite (Changchun Semerete Technology Co., SM-RT-027) [41].

Corneal tissue was rinsed in buffer, post-fixed in 2% osmium tetroxide and 1.5% potassium ferrocyanide in ddH<sub>2</sub>O for 2 h, dehydrated in increasing concentrations of ethanol from 30% to 95% for 5 min each at 48°C. Finally, dehydration embedded in epoxy resin medium (Ted Pella, GP18010). Ultrathin sections were cut with a diamond knife, stained with 5% uranyl acetate and lead citrate, and then observed using transmission electron microscopy.

### Analysis of gene expression

Total RNA of corneal fibroblasts was isolated using TRIzol reagent (OMEGA bio-tek, R6830-01). RNA was treated with gDNA wiper Mix (Vazyme, R223-01) to remove the contaminated genomic DNA and transcribed into cDNA using the HiScript<sup>®</sup> II Q RT SuperMix (Vazyme, R223-01). Quantitative real-time PCR (RT-qPCR) was performed using AceQ<sup>®</sup> qPCR Probe Master Mix (Vazyme, Q112-02/03) with specific primers (Table S2). The mRNA levels of *GAPDH* were used to normalize the expression of genes of interest. Relative quantification based on the  $2^{-\Delta\Delta C_t}$  method was performed to compare the transcript levels of target genes.

### Proteomic analysis

WT and MT corneal fibroblasts were collected and dissolved in lysis buffer (8 M urea [Amresco, M123], 1% Protease Inhibitor Cocktail [Roche, 04693123001]). To digest the protein samples, the protein solution was treated with dithiothreitol, alkylated with iodoacetamide, and then hydrolyzed with trypsin (Promega, V5280). After that, peptide was obtained, and was desalted, vacuum-dried, and

finally reconstituted in TEAB (Sigma-Aldrich, T7408). The tryptic peptides were fractionated by HPLC fractionation and subjected to NSI source followed by tandem mass spectrometry (MS/MS) in Q Exactive<sup>™</sup> Plus (Thermo Fisher Scientific) coupled online to the UPLC. The resulting data of MS/MS was processed using MaxQuant with integrated Andromeda search engine (v.1.5.2.8) [42]. To analyze these data, a volcano plot and a heat map were produced to better visualize and identify the differentially expressed proteins. We also used a subcellular localization prediction software (<http://cello.life.nctu.edu.tw/>) to predict subcellular localization and draw the differentially expressed protein-protein interaction network.

### Ubiquitin modification and western blotting analysis

Total proteins were extracted from corneal fibroblasts using radio-immunoprecipitation assay buffer (Beyotime, P0013B) containing 1% PMSF (Beyotime, ST506). Crude cell lysates were centrifuged at 12,000 g for 10 min at 4°C and protein concentrations were determined via the Bradford method (Beyotime, P0006). Nuclear and cytoplasmic Protein samples of corneal fibroblasts were prepared via a Nuclear and Cytoplasmic Protein Extraction Kit (Beyotime, P0027). Samples were denatured with 5 × loading buffer (Beyotime, P0015), boiled for 4 min at 100°C, and separated by electrophoresis on 12.5% SDS-PAGE gel (EpiZyme, PG113) running continuously at 80 V and 120 V. After electrophoresis, the proteins were transferred onto polyvinylidene difluoride membranes (Millipore Corp, ISEQ00010), that were blocked at room temperature in 8% skim milk (Biofroxx, 1172 GR100) for 2 h and then washed, being incubated with primary antibodies and then the protein post-translational ubiquitin modification and autophagy-related proteins were analyzed. Membranes were washed in PBST (1 × PBS [Hyclone, SH30256.01] containing 0.05% TWEEN-20 [Solarbio, T8220]) three times, followed by incubation with secondary antibody for 1 h at room temperature. The immunoreactive bands were visualized using enhanced Tanon imaging system (Tanon 4600, China) and infrared fluorescence scanning imaging system (Odyssey CLx 1594, USA) and analyzed by ImageJ software version 1.46 r (Wayne Rasband, National Institute of Health, USA), corrected by background subtraction and normalized to the intensity of the corresponding *GAPDH* (glyceraldehyde-3-phosphate dehydrogenase) protein bands.

### Treatment of cells with bafilomycin A<sub>1</sub> and torin 1

The autophagy inhibitors bafilomycin A<sub>1</sub> and torin 1 were first dissolved in dimethyl sulfoxide (TCl, D0798) and then freshly diluted in F-12 culture medium at 0.01 to 0.06 μM and 500 nM, respectively, for use.

### LysoTracker labeling and FC

To visualize enlarged lysosomes, we used LysoTracker, which can stain cellular acidic compartments in lysosomes. Corneal fibroblasts were stained with LysoTracker Green according to



the manufacturer's instructions, then immunofluorescence analysis was conducted by confocal microscopy and the proportion of LysoTracker-positive cells were measured using an FC (Beckman Coulter. Cytomics FC 500MCL).

### Animal experiments

The animal experiments were approved by the Experimental Animal Care Committee of the First Affiliated Hospital of Harbin Medical University. *Tgfb1*-p.Gly623\_Tyr626del transgenic mice were generated with C57BL/6 mice via the CRISPR-Cas9 system with *Tgfb1* gene c.1867–1878 GTGTGGTCTATG del. Two sgRNA sequences were designed (sgRNA 1: GGCATAGACCACACCGTTTGTGG; sgRNA 2: GATGATGGCCACAAACGGTGTGG) and transcribed to target exon 14 in *Tgfb1*. SgRNA, Cas9 as well as donor oligonucleotides were injected into mouse zygotes. *Tgfb1*-p.Gly623\_Tyr626del knock-out heterozygous founders (F0) were obtained and confirmed by DNA sequencing to carry the designated substitute mutations. To assess the genotype of the offspring mice, the examination was performed on DNA extracted from the mice via PCR using the Forward primer: GAGGGTAAGAATCCAGCTAATTGC and Reverse primer: GATAGCCTCAAGTTCTGTAGCATG.

### Statistical analysis

All experimental data were analyzed using Prism 8 version 1.0 (GraphPad, USA). The data given in the text were representatives from at least three independent experiments and performed by Student's t-test.

### Acknowledgments

We thank the department of genetics for their expertise consulting and assistance and the department of rheumatology lab staff for their technical and equipment support.

### Disclosure statement

No potential conflict of interest was reported by the author(s).

### Funding

This study was supported by the Heilongjiang provincial colleges and universities basic scientific research fund (Grant No. 2018-KYYWF-0484), the Heilongjiang Doctor Fund (Grant No. 2020B03), and the Heilongjiang Postdoctoral fund (Grant No. LBH-Z18185).

### Ethics approval

The animal trial was approved by the Medical Ethics Committee of the First Affiliated Hospital of Harbin Medical University (No.2020057).

### ORCID

Liyuan Wang  <http://orcid.org/0000-0001-5273-5197>

Chuchu Zhao  <http://orcid.org/0000-0001-5703-9246>

Tao Zheng  <http://orcid.org/0000-0002-1820-1762>

### References

- [1] Luzio JP, Pryor PR, Bright NA. Lysosomes: fusion and function. *Nat Rev Mol Cell Biol.* 2007;8(8):622–632.
- [2] Ballabio A, Bonifacino JS. Lysosomes as dynamic regulators of cell and organismal homeostasis. *Nat Rev Mol Cell Biol.* 2020;21(2):101–118.
- [3] Finkbeiner S. The autophagy lysosomal pathway and neurodegeneration. *Cold Spring Harb Perspect Biol.* 2020;12(3):a033993.
- [4] Zhang T, Xu D, Poon CY, et al. Tuning the pKa of two-photon bis-chromophoric probes for ratiometric fluorescence imaging of acidic pH in lysosomes. *Talanta.* 2019;202:34–41.
- [5] Seema P, Ahmad H, El-Seedi HR, et al. Cathepsins: proteases that are vital for survival but can also be fatal. *Biomed Pharmacother.* 2018;105:526–532.
- [6] Marques ARA, Di Spiezio A, Thießen N, et al. Enzyme replacement therapy with recombinant pro-CTSD (cathepsin D) corrects defective proteolysis and autophagy in neuronal ceroid lipofuscinosis. *Autophagy.* 2020;16(5):811–825.
- [7] Follo C, Castino R, Nicotra G, et al. Folding, activity and targeting of mutated human cathepsin D that cannot be processed into the double-chain form. *Int J Biochem Cell Biol.* 2007;39(3):638–649.
- [8] Settembre C, Medina DL. TFEB and the CLEAR network. *Methods Cell Biol.* 2015;126:45–62.
- [9] Palmieri M, Impey S, Kang H, et al. Characterization of the CLEAR network reveals an integrated control of cellular clearance pathways. *Hum Mol Genet.* 2011;20(19):3852–3866.
- [10] Settembre C, Zoncu R, Medina DL, et al. A lysosome-to-nucleus signalling mechanism senses and regulates the lysosome via mTOR and TFEB. *EMBO J.* 2012;31(5):1095–1108.
- [11] Roczniak-Ferguson A, Petit CS, Froehlich F, et al. The transcription factor TFEB links mTORC1 signaling to transcriptional control of lysosome homeostasis. *Sci Signal.* 2012;5(228):ra42.
- [12] Martina JA, Chen Y, Gucek M, et al. mTORC1 functions as a transcriptional regulator of autophagy by preventing nuclear transport of TFEB. *Autophagy.* 2012;8(6):903–914.
- [13] Medina DL, Di Paola S, Peluso I, et al. Lysosomal calcium signalling regulates autophagy through calcineurin and TFEB. *Nat Cell Biol.* 2015;17(3):288–299.
- [14] Boutboul S, Black GC, Moore JE, et al. A subset of patients with epithelial basement membrane corneal dystrophy have mutations in *TGFBI/BIGH3*. *Hum Mutat.* 2006;27(6):553–557.
- [15] Hashimoto K, Noshiro M, Ohno S, et al. Characterization of a cartilage-derived 66-kDa protein (RGD-CAP/beta ig-h3) that binds to collagen. *Biochim Biophys Acta.* 1997;1355(3):303–314.
- [16] Billings PC, Herrick DJ, Kucich U, et al. Extracellular matrix and nuclear localization of beta ig-h3 in human bladder smooth muscle and fibroblast cells. *J Cell Biochem.* 2000;79(2):261–273.
- [17] Kim JE, Kim SJ, Jeong HW, et al. RGD peptides released from beta ig-h3, a TGF-beta-induced cell-adhesive molecule, mediate apoptosis. *Oncogene.* 2003;22(13):2045–2053.
- [18] Kim MO, Yun SJ, Kim IS, et al. Transforming growth factor-beta-inducible gene-h3 (beta ig-h3) promotes cell adhesion of human astrocytoma cells in vitro: implication of alpha6beta4 integrin. *Neurosci Lett.* 2003;336(2):93–96.
- [19] Weiss JS, Møller HU, Aldave AJ, et al. IC3D classification of corneal dystrophies—edition 2 [published correction appears in *Cornea.* 2015 Oct;34(10):e32]. *Cornea.* 2015;34(2):117–159.
- [20] Nielsen NS, Poulsen ET, Lukassen MV, et al. Biochemical mechanisms of aggregation in *TGFBI*-linked corneal dystrophies. *Prog Retin Eye Res.* 2020;77:100843.

- [21] Niel-Buttschi F, Kantelip B, Iwaszkiewicz J, et al. Genotype-phenotype correlations of *TGFBI* p.Leu509Pro, p.Leu509Arg, p.Val613Gly, and the allelic association of p.Met502Val-p.Arg555Gln mutations. *Mol Vis*. 2011;17:1192–1202.
- [22] Munier FL, Frueh BE, Othenin-Girard P, et al. BIGH3 mutation spectrum in corneal dystrophies. *Invest Ophthalmol Vis Sci*. 2002;43(4):949–954.
- [23] Munier F, Korvatska E, Djemai A, et al. Kerato-epithelin mutations in four 5q31-linked corneal dystrophies. *Nat Genet*. 1997;15(3):247–251.
- [24] Soh YQ, Kocaba V, Weiss JS, et al. Corneal dystrophies. *Nat Rev Dis Primers*. 2020;6(1):46.
- [25] Nakamura H, Li FT, Foltermann MO, et al. Individual phenotypic variances in a family with Thiel-Behnke corneal dystrophy. *Cornea*. 2012;31(11):1217–1222.
- [26] Choi SI, Kim BY, Dadakhujaev S, et al. Impaired autophagy and delayed autophagic clearance of transforming growth factor  $\beta$ -induced protein (TGFBI) in granular corneal dystrophy type 2. *Autophagy*. 2012;8(12):1782–1797.
- [27] Ciechanover A. Proteolysis: from the lysosome to ubiquitin and the proteasome. *Nat Rev Mol Cell Biol*. 2005;6(1):79–87.
- [28] Chazotte B. Labeling lysosomes in live cells with LysoTracker. *Cold Spring Harb Protoc*. 2011;2011(2):pdb.prot5571.
- [29] Blázquez M, Shennan KI. Basic mechanisms of secretion: sorting into the regulated secretory pathway. *Biochem Cell Biol*. 2000;78(3):181–191.
- [30] Mathivanan S, Ji H, Simpson RJ. Exosomes: extracellular organelles important in intercellular communication. *J Proteomics*. 2010;73(10):1907–1920.
- [31] Karring H, Runager K, Valnickova Z, et al. Differential expression and processing of transforming growth factor beta induced protein (TGFBIP) in the normal human cornea during post-natal development and aging. *Exp Eye Res*. 2010;90(1):57–62.
- [32] Napolitano G, Ballabio A. TFEB at a glance. *J Cell Sci*. 2016;129(13):2475–2481.
- [33] Settembre C, Fraldi A, Medina DL, et al. Signals from the lysosome: a control centre for cellular clearance and energy metabolism. *Nat Rev Mol Cell Biol*. 2013;14(5):283–296.
- [34] Palmieri M, Pal R, Nelvagal HR, et al. mTORC1-independent TFEB activation via Akt inhibition promotes cellular clearance in neurodegenerative storage diseases [published correction appears in *Nat Commun*. 2017 Jun 13;8:15793]. *Nat Commun*. 2017;8:14338.
- [35] Lee BH, Bae JS, Park RW, et al.  $\beta$ ig-h3 triggers signaling pathways mediating adhesion and migration of vascular smooth muscle cells through  $\alpha$ v $\beta$ 5 integrin. *Exp Mol Med*. 2006;38(2):153–161.
- [36] Huang Y, Chen Y, Shaw AM, et al. Enhancing TFEB-mediated cellular degradation pathways by the mTORC1 inhibitor quercetin. *Oxid Med Cell Longev*. 2018;2018:5073420.
- [37] Liu Z, Chen D, Chen X, et al. Trehalose induces autophagy against inflammation by activating TFEB signaling pathway in human corneal epithelial cells exposed to hyperosmotic stress. *Invest Ophthalmol Vis Sci*. 2020;61(10):26.
- [38] Zheng X, Chu F, Mirkin BL, et al. Role of the proteolytic hierarchy between cathepsin L, cathepsin D and caspase-3 in regulation of cellular susceptibility to apoptosis and autophagy. *Biochim Biophys Acta*. 2008;1783(12):2294–2300.
- [39] Yamazoe K, Yoshida S, Yasuda M, et al. Development of a transgenic mouse with R124H human *TGFBI* mutation associated with granular corneal dystrophy type 2. *PLoS One*. 2015;10(7):e0133397.
- [40] Kitamoto K, Taketani Y, Fujii W, et al. Generation of mouse model of *TGFBI*-R124C corneal dystrophy using CRISPR/Cas9-mediated homology-directed repair. *Sci Rep*. 2020;10(1):2000.
- [41] Saheli M, Sepantafar M, Pournasr B, et al. Three-dimensional liver-derived extracellular matrix hydrogel promotes liver organoids function. *J Cell Biochem*. 2018;119(6):4320–4333.
- [42] Cox J, Mann M. MaxQuant enables high peptide identification rates, individualized p.p.b.-range mass accuracies and proteome-wide protein quantification. *Nat Biotechnol*. 2008;26(12):1367–1372.